EFFECTS OF THICKNESS DIFFERENCE AND LOADING DIRECTION ON FATIGUE PROPERTIES OF TAILORED WELDED BLANKS

ANGELINA ANAK LAWRENCE

Bachelor of Mechanical Engineering
UNIVERSITI MALAYSIA PAHANG

ANGELINA ANAK LAWRENCE MA09041 BACHELOR OF MECHANICAL ENGINEERING

FFECTS OF THICKNESS DIFFERENCE AND LOADING DIRECTION ON FATIGUE PROPERTIES OF TAILORED WELDED BLANKS

ANGELINA ANAK LAWRENCE

UNIVERSITI MALAYSIA PAHANG

EFFECTS OF THICKNESS DIFFERENCE AND LOADING DIRECTION ON FATIGUE PROPERTIES OF TAILORED WELDED BLANKS

ANGELINA ANAK LAWRENCE

Thesis submitted in fulfillment of the requirements
for the award of the degree of
Bachelor of Mechanical Engineering

Faculty of Mechanical Engineering
UNIVERSITI MALAYSIA PAHANG

JUNE 2013

EXAMINER'S DECLARATION

I certify that the thesis entitled "Effect of Thickness Difference and Loading Direction on Fatigue Properties of Tailored Welded Blanks" is written by Angelina Anak Lawrence. I have examined the final copy of this report and in my opinion, it is fully adequate in terms of language standard, and report formatting requirement for the award of the degree of Bachelor of Mechanical Engineering. I herewith recommend that it will be accepted fulfillment of the requirements for the degree of Bachelor of Mechanical Engineering.

Signature:
Name of Supervisor: IR. MOHD RASHIDI MAAROF
Position: LECTURER
Date: JUNE 2013

SUPERVISOR'S DECLARATION

I hereby declare that I have checked this thesis and in my opinion, this thesis is adequate in terms of scope and quality for the award of the degree of Bachelor of Mechanical Engineering.

Signature:	
Name of Supervisor:	DR. SITI RABIATULL AISHA BINTI IDRIS
Position:	LECTURER
Date:	JUNE 2013

STUDENT'S DECLARATION

I hereby declare that the work in this thesis is my own except for quotations and summaries which have been duly acknowledged. The thesis has not been accepted for any degree for any degree and is not concurrently submitted for award of other degree.

Signature

Name:	ANGELINA ANAK LAWRENCE
ID Number:	MA09041
Date:	JUNE 2013

Dedicated to my beloved parents;

Mr. Lawrence Kiang ak Panger

Mrs. Lily ak Diye

dearest family members and friends;

without their lifetime supports, my pursuit of higher education would not have been possible.

Thank you so much.

ACKNOWLEDGEMENTS

I am grateful and would like to express my sincere gratitude to my supervisor Dr Rabiatull Aisha for her excellent ideas, invaluable guidance, continuous support and encouragement in making this research possible. I appreciate for her time spent and efforts throughout the study.

My sincere thanks go to all staff of the Faculty of Mechanical Laboratory who gave the permissions to use all required machinery and the necessary material to complete the study. I would like to thank for their comments, time spent and knowledge on the study during the project was carried out. Many special thanks go to all focus group members for their co-operation and supports during this study. Also, I would like to appreciate the suggestions and comments given by other supervisor and panels in correcting my many mistakes.

I acknowledge my sincere gratitude to my parents for their love, dream and sacrifice throughout my life. I am very thankful to my family members and friends for their support and encouragement under all circumstances.

Last but not least, above all, to Almighty God for giving me good health, strength and perseverance to carry out this research.

ABSTRACT

An approach to reduce manufacturing cost, weight, design and improve quality of a component is through the use of tailor welded blanks (TWBs). TWBs are welded blanks that consist of similar or dissimilar material, thicknesses, and surface properties before forming process. The purpose of the project is to evaluate the strength and fatigue behavior of the TWBs with different thickness combination and loading direction. The welding process was done by tungsten inert gas (TIG) arc welding. This study is divided into three parts. First, tensile tests were carried out. It was found that combinations were affected by the difference in thickness (2 mm/3 mm) and weld orientation (45^o and 90^o towards loading direction). The failure occurred in the middle of the weaker base metal parts. However, some of the joint specimens broke at the heat-affected zone. In addition, weld loading direction played a dominant role when the thickness difference was large. The second part investigates the effect of welding joint on the fatigue strength of the TWBs combination. The experimental results show that the failure occurs at welding zone as the specimens were subjected to fatigue and impact loading. In the last part of this thesis, the examination of the weld quality was carried out. Through the microstructure constituents in the weld, the strength and effects on the TWBs were discussed.

ABSTRAK

Sebuah pendekatan dalam mengurangkan kadar kos pengeluaran, berat, reka bentuk dan peningkatan kualiti dalam sebuah komponen ialah melalui penggunaan *tailor welded blanks (TWBs*). *TWB* merupakan kimpalan kosong yang melibatkan penggunaan bahan yang sama atau berlainan, beza ketebalan dan sifat-sifat pada permukaan sebelum proses membentuk. Tujuan projek ini dilaksanakan ialah untuk menilai kekuatan dan sifat kelesuan kimpalan kosong yang terdiri daripada ketebalan yang berbeza dan arah beban. Proses kimpalan dilakukan dengan mengguna *gas tungsten arc welding(GTAW)*. Kajian ini merangkumi tiga bahagian. Pertama sekali, ujian tegangan dijalankan. Kajian ini mendapati sambungan *TWBs* dijejaskan oleh perbezaan ketebalan (2 mm/3 mm) serta orientasi semasa mengimpal (45^{o} dan 90^{o} ke arah beban). Kegagalan berlaku di bahagian tengah logam yang lemah. Namun, sesetengah sambungan kimpalan patah di *heat affected zone* (*HAZ*). Selain itu, arah beban memainkan peranan yang dominan apabila perbezaan ketebalan besar. Bahagian kedua tesis mengkaji kesan sambungan *TWBs* terhadap kekuatan kelesuan. Ujian eksperimen menunjuk bahawa kegagalan berlaku di zon kimpalan di mana specimen tertakluk kepada keletihan dan kesan beban. Bahagian terakhir tesis ini ialah pemeriksaan kualiti kimpalan.Melalui pembentukan juzuk mikrostruktur yang terdapat di dalam kimpalan, kekuatan dan kesannya terhadap *TWBs* telah dibincangkan.

TABLE OF CONTENTS

	Page
EXAMINER'S DECLARATION	ii
SUPERVISOR'S DECLARATION	iii
STUDENT'S DECLARATION	iv
DEDICATION	v
ACKNOWLEDGEMENTS	vi
ABSTRACT	vii
ABSTRAK	viii
TABLE OF CONTENTS	ix
LIST OF TABLES	xii
LIST OF FIGURES	xiii
LIST OF SYMBOLS	xvi
LIST OF ABBREVIATIONS	xvii

CHAPTER 1 INTRODUCTION

1.1	General Background		1
1.2	Problem Statement		1
1.3	Objectives		2
1.4	Scopes		2

CHAPTER 2 LITERATURE REVIEW

2.1	Introduction		4
2.2	TWB		4
2.3	Welding Processes		5
	2.3.1	TIG Welding	5
	2.3.2	MIG Welding	6
	2.3.3	Weld Quality	7
	2.3.4	Weldability	8
2.4	Material Properties		8
	2.4.1	Steel Alloy TWBs	8

2.4.2 Aluminum Alloy TWBs 9
2.4.3 Summary 9

2.5 Formability of Tailored Welded Blanks 10

2.5.1 Thickness Difference 10
2.5.2 Summary 15
2.5.3 Loading Direction 16
2.5.4 Summary 17

2.6 Fatigue of Tailored Welded Blanks 17

2.6.1 Summary 19

CHAPTER 3 METHODOLOGY

3.1 Introduction 21

3.2 Flow Chart Description 22

3.2.1 Literature Review 23
3.2.2 Design of Experiment 23
3.2.3 Specimen Preparation 23
3.2.4 Welding 29
3.2.5 Testing 33
3.2.6 Characterization 37
3.2.7 Preliminary Result 42
3.2.8 Presentation and Documentation 44
3.2.9 Gantt Chart 44

CHAPTER 4 RESULTS AND DISCUSSION

4.1 Introduction 45

4.2 Material Composition 45

4.3 Weld Quality 46

4.4 Tensile Test 48

4.5 Fatigue Test 51

4.6 Microstructure Test 54

4.7 SEM 61

CHAPTER 5 CONCLUSION AND RECOMMENDATION

5.1 Conclusions 64

5.2 Recommendation 65

REFERENCES 66

APPENDICES

A1 70

A2 71

A3 72

A4 73

A5 74

A6 75

LIST OF TABLES

Table No.	Title	Page
Table 3.1	Composition of 1045 medium carbon steel	24
Table 3.2	Parameters for turning operation	27
Table 3.3	TIG welding parameters	30
Table 3.4	Welding specifications	30
Table 3.5	Parameters used for surface grinding stage	38
Table 3.6	Parameters used for surface polishing stage	38
Table 4.1	Chemical composition of the material	46
Table 4.2	The tensile test data collection	49
Table 4.3	Failure location and orientation in the specimens	50

LIST OF FIGURES

Figure No.	Title	Page
Figure 2.1	Various tailor-welded blank components used in an automotive structure	5
Figure 2.2	TIG welding process works	6
Figure 2.3	MIG welding process works	7
Figure 2.4	A TWB structure with different material regions and Thicknesses	10
Figure 2.5	Two types of splitting in forming of TWBs	11
Figure 2.6	LDH values of TWBs with different thickness ratio	12
Figure 2.7	Variety of forming limit strains in a FLD	12
Figure 2.8	Comparing the FLDs level of TWBs of different thickness ratio	13
Figure 2.9	Comparing the FLDs of TWBs of different thickness ratio with the base metal of thickness 1 mm	14
Figure 2.10	Failure mode of TWBs	17
Figure 2.11	Fatigue test results for laser and spot weld	18
Figure 3.1	Project flow chart	22
Figure 3.2	General view of a Sodick AQ535L Wire Cut Machine, showing various components	25
Figure 3.3	Finished machining of tensile specimen	25
Figure 3.4	General view of a Pinacho S 90VS/180 Conventional lathe machine, showing various components	28
Figure 3.5	Raw materials of medium carbon steels	28
Figure 3.6	Turning process of conventional lathe machine	29
Figure 3.7	Finished machining fatigue specimen	29
Figure 3.8	Tensile test welding specifications	30

Figure 3.9	A Syncrowave 200 Miller TIG welding machine	31
Figure 3.10	Cross section view during TIG welding	31
Figure 3.11	The completed end view weldment	32
Figure 3.12	Butt joint TWBs combination	32
Figure 3.13	Welded specimen for (a) tensile specimen and (b) fatigue Specimen	33
Figure 3.14	General view of an Instron Universal Tensile Testing Machine Model 3369, showing various components	35
Figure 3.15	General view of a WP 140 Fatigue Testing Apparatus, showing various components	36
Figure 3.16	Components of inverted microscope	40
Figure 3.17	IM7000 Series Inverted Microscope	41
Figure 3.18	Scanning Electron Microscopy EVO®50 02-73	42
Figure 3.19	Stress strain diagram	43
Figure 3.20	SN curve diagram	43
Figure 4.1	Various forms of welding defects: (a) spatters, (b) cracks, (c) incomplete fills, and (d) cavities	47
Figure 4.2	Schematic of TWBs after the tensile test: (a) Same thickness, t=2 mm with 90 ^{o} orientation; (b) Same thickness, t=2 mm with 45 ^{o} orientation; (c) Same thickness, t=3 mm with 90 ^{o} orientation; (d) Same thickness, t=3 mm with 45 ^{o} orientation; (e) Different thickness, t=2 mm & 3 mm with 90 ^{o} orientation; (f) Different thickness, t=2 mm & 3 mm with 45 ^{o} orientation	48
Figure 4.3	Cross section on TWB after tensile test	50
Figure 4.4	S-N curves for the TWB combinations	52
Figure 4.5	Log-log S-N curve	52
Figure 4.6	Fatigue crack surface	54
Figure 4.7	Cross section of weld joints	54

Figure 4.8	Micrographs showing the microstructure change in medium carbon steel joints before etching for different thickness of TWBs combination (a) base metal, (b) weld zone, and (c) HAZ	56
Figure 4.9	Micrographs showing the microstructure change in medium carbon steel joints before etching for same thickness of TWBs combination (a) base metal, (b) weld zone, and (c) HAZ	57
Figure 4.10	Micrographs showing the microstructure change in medium carbon steel joints after etching for same thickness TWB combination (a) base metal, (b) weld zone, and (c) HAZ	59
Figure 4.11	Micrographs showing the microstructure change in medium carbon steel joints after etching for different thickness TWB combination (a) base metal, (b) weld zone, and (c) HAZ	60
Figure 4.12	Cross section of the fracture specimen	61
Figure 4.13	Typical SEM images of fatigue fracture surface (a) rough surface area, (b) smooth surface area, (c) transition zone, (d) HAZ and (e) defects	63

LIST OF SYMBOLS

N	Spindle speed
CS	Cutting speed
d	Work piece diameter
v_f	Feed rate
f	Feed
σ	Engineering stress
ϵ	Engineering strain
E	Modulus of elasticity

LIST OF ABBREVIATIONS

TWB	Tailor welded blank
TIG	Tungsten inert gas
MIG	Metal inert gas
GTAW	Gas tungsten arc welding
GMAW	Gas metal arc welding
LDH	Limiting dome height
FLD	Forming limit diagram
SEM	Scanning Electron Microscope
HAZ	Heat affected zone
EDM	Electrode Discharge Machine
ASTM	American Society for Testing and Materials
SAE	Society of Automotive Engineers
AISI	American Iron and Steel Institute

CHAPTER 1

INTRODUCTION

1.1 GENERAL BACKGROUND

The project concerned on the experiment that is to determine the effect of thickness ratio and loading direction on fatigue properties of tailor welded blanks (TWBs). To imitate the actual TWB panels, method of welding two small panels with different thickness and loading direction are done. Two tests are conducted that is fatigue and tensile test. Fatigue properties are an integral part of materials comparison activities and offer information for structural life estimation. Fatigue test is conducted in a rotating bending stress with constant amplitude until the specimen failed. A fatigue failure usually originates at a point of stress concentration such as notch and connecting rods. On the other hand, tensile test reveals the mechanical properties of strength on the welded joints. The welded specimen is pulled to failure in a relatively short time at a constant rate. Fatigue crack propagation and deformation of the specimen analyses were performed in order to discuss the effect on properties of TWB.

1.2 PROBLEM STATEMENT

TWB is a potential process to reduce general weight in automotive parts. It offers an opportunity to reduce weight and overall cost. Formability characteristics of TWBs are affected by weld conditions such as weld properties, weld orientation and weld location, thickness difference and strength difference between the sheets. It has evidence regarding the welded joints due to welding procedure does have influence on fatigue and tensile strength.

However, the effect of thickness ratio and loading direction on the tensile strength on TWB remain unclear. Therefore, the current work will focus on tensile test of specimen with angles of 90 ^{o} and 45 ^{o} to the weld line, in order to clarify the influence of loading directions and different in thickness. Other than that, the fatigue test concern on the fatigue behavior of the welded joints. That method is used to measure fatigue life of the specimen. Through the study, specimens are fabricates using a welding process and procedure depend on the certain thickness and loading direction thus investigate the fatigue and tensile properties of TWB.

1.3 OBJECTIVES

The objectives for this study are:

- To investigate the effect of thickness difference and loading direction on the tensile behavior.
- To evaluate the fatigue strength of the materials used.
- To clarify high quality weld obtained by using tungsten inert gas (TIG) welding.
- To define the microstructures on the welded joints.

1.4 SCOPES

The scopes of project are explained in detail as below:

- 1045 medium carbon steel is used.
- TIG butt joint welding with parameter 45 A and 13 V are used.
- Fatigue test is conducted to investigate the fatigue behavior of welded joints. The maximum value F= 250 N is used as the initial measure to get the number of load cycles.
- Tensile test is conducted to investigate the tensile strength of welded joints. The cross head speed applied during the test is 1 mm/min.
- Different thickness (2 mm/3 mm) and loading direction (90 ^{o} and 45 ^{o} towards loading direction) of specimens are prepared for the tensile test.

- The fracture surface is analyzed by using scanning electron microscope (SEM).
- The microstructure constituents in the weldment are analyzed by using optical microscope to distinguish the defects and grain boundaries.

CHAPTER 2

LITERATURE REVIEW

2.1 INTRODUCTION

This chapter will be discussed on the background of study and past research on TWB. The sources of the review are extracted from journals, articles, reference books and internet. The purpose of this section is to provide additional information and relevant facts based on past researches which related to this project. This chapter will cover on background of TWB, welding processes, material properties, formability of TWB, and fatigue test of TWB.

2.2 TWB

TWB involve the welding of two or more sheets together equal or different thickness, strength, loading direction or surface coatings welded before forming process. Alternatively, various steel options can be welded together prior to the forming process to produce a TWB. Such a concept of combining different materials into a welded blank enables engineers to tailor the blank so that appropriate material with the required properties are located precisely within the part where needed. The differences in the materials can be found in their grade, thickness, strength and surface condition. The tailor welded blanks are currently generated most interest in the automotive industry such as for body side frames, door inner panels, motor compartment rails, center pillar, inner panels and wheelhouse as shown in Figure 2.1. TWB have been found to have many potential benefits including fewer parts, reduced design, lower manufacturing costs, weight reduction and improved safety (Anand, 2004).

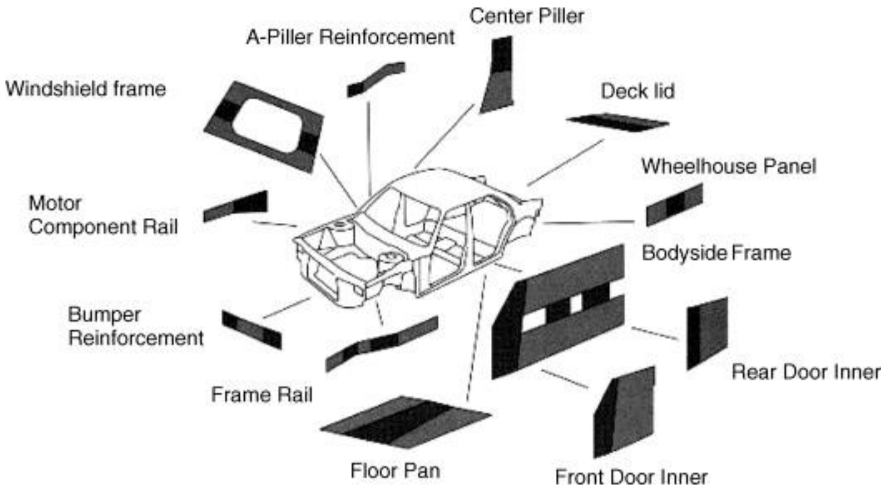

Figure 2.1: Various tailor-welded blank components used in an automotive structure

Source: Anand *et al*. (2006)

2.3 WELDING PROCESSES

There are two most common welding processes which are including TIG and metal inert gas welding (MIG). TIG is also referred to as gas tungsten arc welding (GTAW) while MIG also is referred to as gas metal arc welding (GMAW).

2.3.1 TIG Welding

The arc is started with a tungsten electrode shielded by inert gas and filler rod is fed to the weld puddle separately. The gas shielding that is required to protect the molten metal from contamination and amperage is supplied during the TIG welding operation. TIG welding is a slower process than MIG, but it produces a more precise weld. The reasons for this feature are because TIG has stable and consistent arc. The length of arc also benefits due to arc shape and even heat distribution. It can be used at lower amperages for thinner metal and even on exotic metals. TIG welding has became the most choice of welding processes due to high quality welding process and thus precision welding is required (Mendez, 2000). Besides, TIG welding process requires more time to learn than MIG. In TIG welding, an arc is formed between a non-consumable tungsten electrode and the metal was welded. Gas is fed through the torch to shield the electrode and molten weld pool. If filler wire is used, it is added to the weld pool separately. The TIG welding process utilizes a number of shielding gases including argon, helium and combination of argon with helium. The illustration in Figure 2.2 provides a schematic showing how the TIG welding process works.

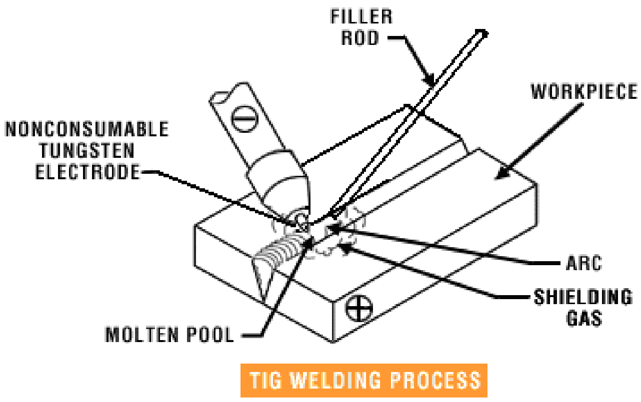

Figure 2.2: TIG welding process works

Source: Articles on Advantage Fabricated Metals (2009)

2.3.2 MIG Welding

The wire that is used to start the arc is referred as the metal in MIG welding. It is shielded by inert gas and the feeding wire also acts as the filler rod. MIG is fairly easy to learn and use as it is semi-automatic welding process. During the MIG welding process, the electrode melts within the arc and becomes deposited as filler material. The shielding gas that is used prevents atmospheric contamination and protects the weld during solidification. The shielding gas also assists with stabilizing the arc which provides a smooth transfer of metal from the weld wire to the molten weld pool. Versatility is the major benefit of the MIG welding process. It is capable of joining most types of metals and it can be performed in most positions, even though flat horizontal is most suitable. MIG is used to weld many materials and different gases are used to form the arc depending on the materials to be welded together. The illustration in Figure 2.3 provides a look at a typical MIG welding process showing an arc that is formed between the wire electrode and the work piece (Andrews, 2008).

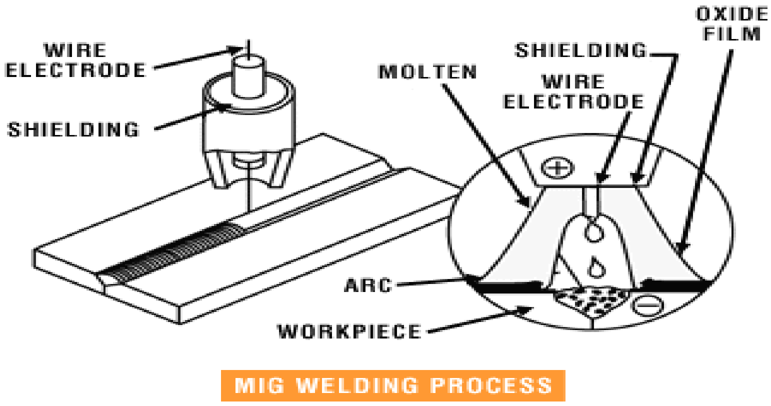

Figure 2.3: MIG welding process works

Source: Articles on Advantage Fabricated Metals (2009)

2.3.3 Weld Quality

The purpose of welding process is to join two or more components into a single structure. The structure formed depends on the quality of the weld. The discussion was covered on the weld quality deals with arc welding. The rapid heating and cooling in localized regions of the work during fusion welding cause residual stresses in the weldment due to the thermal expansion and contraction. The materials are heated to high themperature, usually more than 1200 ^{o}C and faced intermediate cooling rate generally employed 10 to 200 ^{o}C/min, gives great loss in impact strength. Later, these stresses cause distortion and warping of the welded assembly. In addition to residual stresses and distortion in the assembly, other defects such as voids and cracks also occur in welding.

There is a variety of inspection and testing methods are available to check the quality of the welded joint. Other type of testing method is known as destructive testing in which the weld is destroyed either during the test or to prepare the test specimen. They include mechanical and metallurgical tests. Mechanical test is more likely to conventional testing method such as tensile test. However, the difference is that the test specimen is a welded blank. Metallurgical test involves the preparation of metallurgical specimens of the weldment to examine such features like metallic structure, defects, condition of heat-affected zone and presence of other elements.

2.3.4 Weldability

Weldability is the capacity of a metal or combination of metals to be welded into an assembled blank and for the resulting weld joint to posses the required metallugical properties. Good weldabilty is characterized by the ease with which the welding process is accomplished, absence of weld defects, and acceptable strength, ductility and toughness in the welded joint. Factors that affect weldability include welding processs, base metal properties, filler metal and surface conditions. Carbon steel can be readily welded by most arc welding processes. Properties of the base metal such as melting point, thermal conductivity and coefficient of thermal expansion affect welding performance. Carbon steel has medium melting point which is quite suitable for welding since it is not melt too easily. Carbon steel has high thermal conductivity that tend to transfe heat away from the weld zone which can make them hard to weld. High thermal expansion in the metal causes distortion problems in the welded blank. Surface condition of the base metal can adversely affect the operation. Moisture or corroded area can result in porosity in the fusion zone.

2.4 MATERIAL PROPERTIES

Nowadays, there are only two major categories of materials that can be considered and widely used to produce TWBs due to the technical capability. The first one is steels and the other one is aluminum alloys. Steel TWBs and aluminum TWBs possess different forming performance and deformation behavior during production of TWB component due to the weldability, formability and mechanical properties (Cheng, 2010).

2.4.1 Steel Alloy TWBs

Steel TWBs have been successfully applied to the production of automotive components for many years. The development of steel TWBs became the priority for making the automotive body structures by incorporating the concept of TWB (Ultra Light Steel Auto Body Consortium, 1998, and Auto/Steel Partnership, 1995). Waddell and Davis (1995) have mentioned that steel TWBs have the advantages such as weight and cost reduction, structural improvement, corrosion resistance improvement and part stiffness.

2.4.2 Aluminum Alloy TWBs

Aluminum alloys have been adopted together with the TWB concept to produce much lighter TWB components for the modern vehicles (Davies *et al.*, 1999). Aluminum and steel can have similar strength values, but since its density is significantly lower (approximately 2.7 g/cm^3 than steel 7.8 g/cm^3), aluminum possesses higher strength to weight ratios. Still, depending on the application, aluminums' weight can save up to 50 % (Tuler, 1999). However, the weld in aluminum TWBs is not typically stronger compare to the base material. When welding, the material around the weld becomes much hotter than 200 ^{o}C, so the material tends to lose some of its strength. It becomes significantly weaker than the rest of the aluminum by as much as 30 to 40 %. Hence, the prevention of failure or strain localization in the weld is more difficult (Cheng, 2005). Weld failure often occurred during the forming process of aluminum TWBs. The establishment of an effective formability analysis with the weldment properties is taking into consideration to predict the forming performance including the weld failure.

2.4.3 Summary

There is a research reported that the forming limit of a TWB depends on the specific welding set-up conditions and the material used. The maximum formability can be achieved by optimizing welding parameters and or by using more formable and very low carbon steels, which result in a more formable weld. So, we can assume that steel alloys are more suitable to formability of tailored welded blanks.

2.5 FORMABILITY OF TAILORED WELDED BLANKS

TWBs are multiple sheets of material which are welded together prior to the forming process. The differences in the material within a TWB can be in the thickness, grade or coating of the material, for example galvanized versus ungalvanized (Panda and Kumar, 2008). The tensile behavior of TWB is affected by various parameters such as thickness ratio, strength, weld conditions including weld properties, orientation, width, location and possibly different in proportions.

2.5.1 Thickness Difference

Several material regions can be classified in a TWB including the base metal sheets with different configurations, welded metal and the adjacent heat-affected zone as shown in Figure 2.4. Each material region possesses its own distinctive material properties and forming limit. According to Shi *et al.* (1993), in the drawing quality steel have been reported different modes of forming failure for TWBs. In a similar thickness TWB combination (0.8-0.8 mm), the failure occurs in a direction perpendicular to the weld bead. In the case of a dissimilar thickness TWB (0.8-1.8 mm), failure occurs in the thinner material and is oriented parallel to the weld bead as shown in Figure 2.5. To obtain the maximum formability performance of TWBs, deformation in the thinner or lower strength material should be minimized.

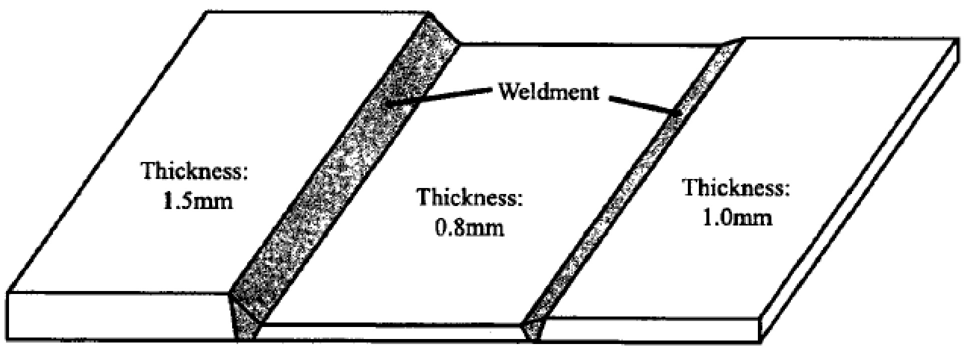

Figure 2.4: A TWB structure with different material regions and thicknesses

Source: Cheng (2010)

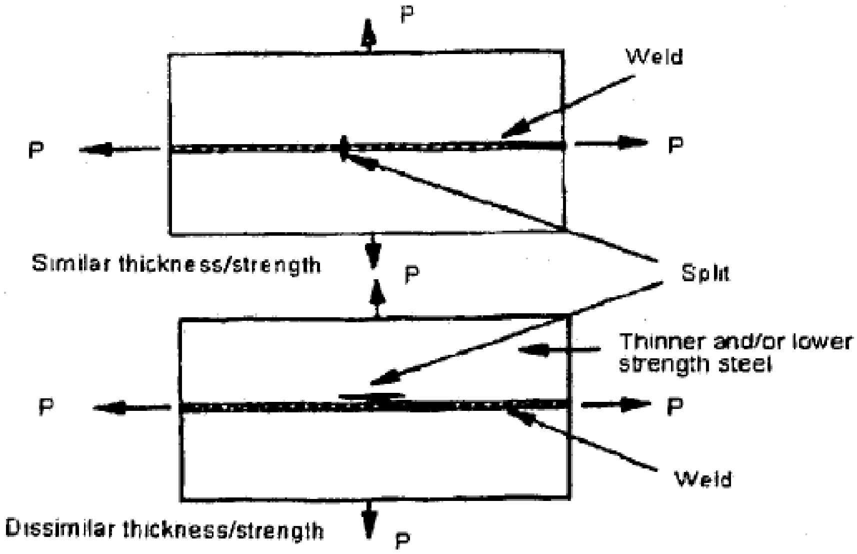

Figure 2.5: Two types of splitting in forming of TWBs

Source: Anand (2004)

Chan *et al.* (2003) reported the effect of varying thicknesses on the formability of the TWBs. An Nd:YAG laser was used for butt welding cold rolled sheets. Their different thickness combinations were 0.5-1.0 mm, 0.6-1.0 mm and 0.8-1.0 mm, having a given carbon content of 0.12 %. The weld beam in the forming tests was oriented perpendicularly to the major strain axis. They evaluated the performance of the TWBs based on the thickness ratio by measuring the limiting dome heights (LDH) to failure. LDH represents the maximum height to which a sheet specimen can stretch at the onset of necking or failure. They reported that the lower the thickness ratio of the TWBs, the higher the LDH values as shown in Figure 2.6. Keeler and Backofen (1963) have proposed a forming limit diagram (FLD) which involved a wide-range of forming limit strains of a homogeneous material at different strain states as illustrated in Figure 2.7. FLD helps to evaluate and predict the forming performances of various sheet metals. Failure of a stretched sheet metal is often characterized by the occurrence of localized necking. After necking, material fracture occurs. By using the localized necking criterion, FLD is defined. Chan *et al.* (2003) has carried out an experiment on the analysis of the FLD of TWBs with different thickness ratios.

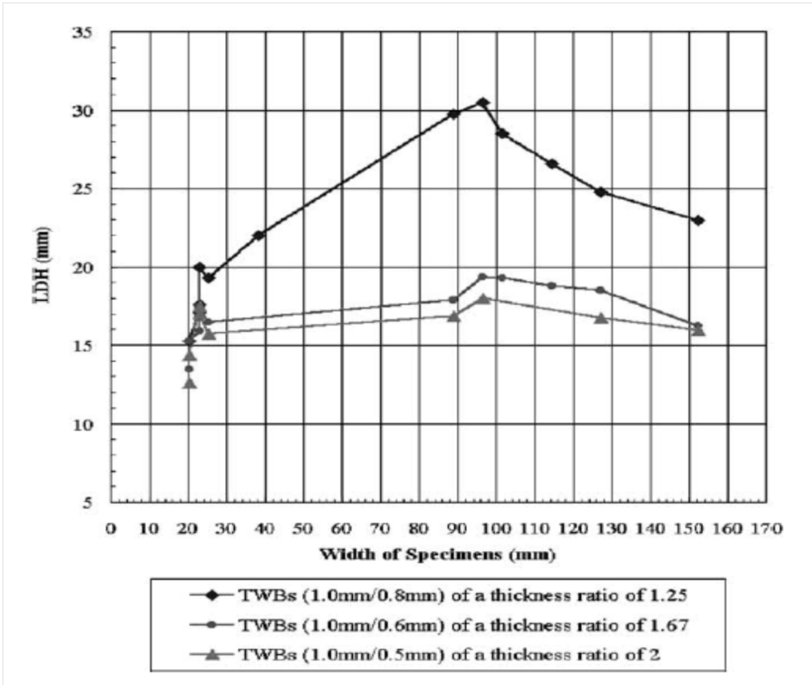

Figure 2.6: LDH values of TWBs with different thickness ratio

Source: Chan *et al*. (2003)

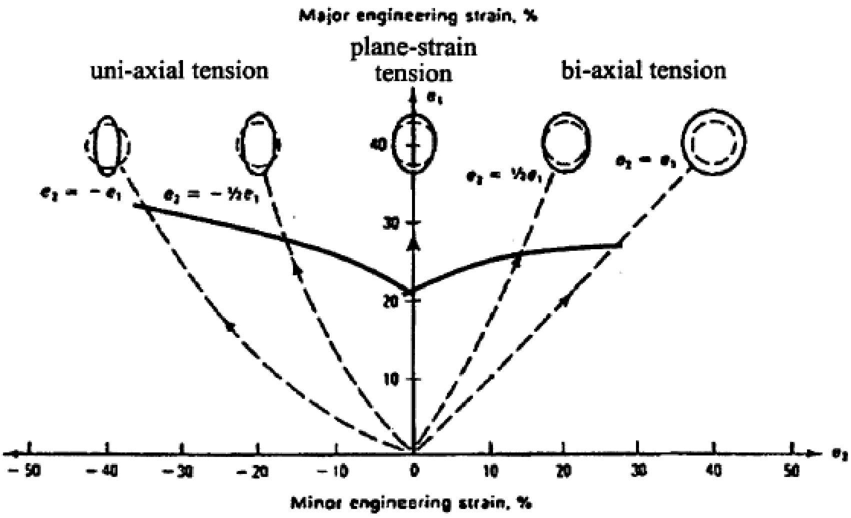

Figure 2.7: Variety of forming limit strains in a FLD

Source: Taylor (1996)

Figure 2.8 shows the FLD of TWBs of different thickness ratios. It was found that the TWBs having the highest thickness ratio yield the lowest FLD value. A higher thickness ratio implies a large difference of plastic deformation during forming. Figure 2.9 shows the comparison between the FLD of the base metals of thickness 1 mm with the TWBs. The FLD value of the TWBs was reported to be lower than the FLD of the thicker base metal, which indicates that the TWBs have a lower strength against deformation during the forming process.

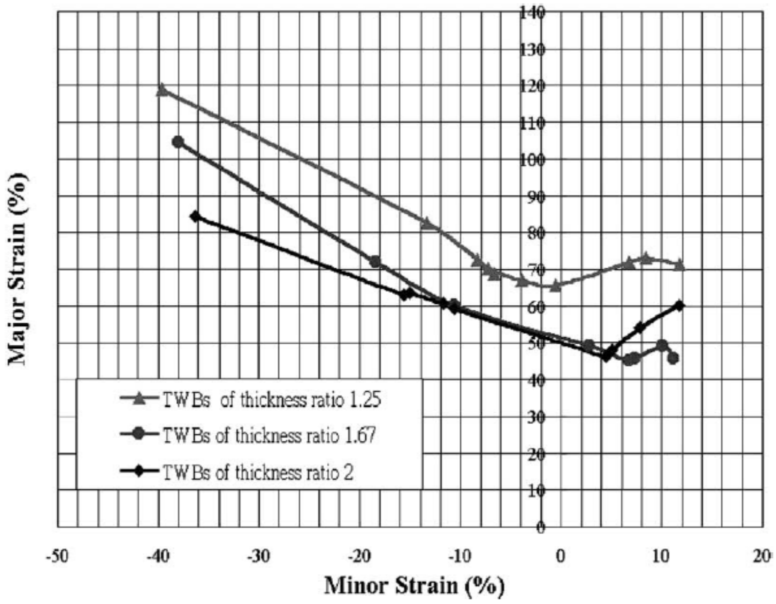

Figure 2.8: Comparing the FLDs level of TWBs of different thickness ratio

Source: Chan *et al*. (2003)

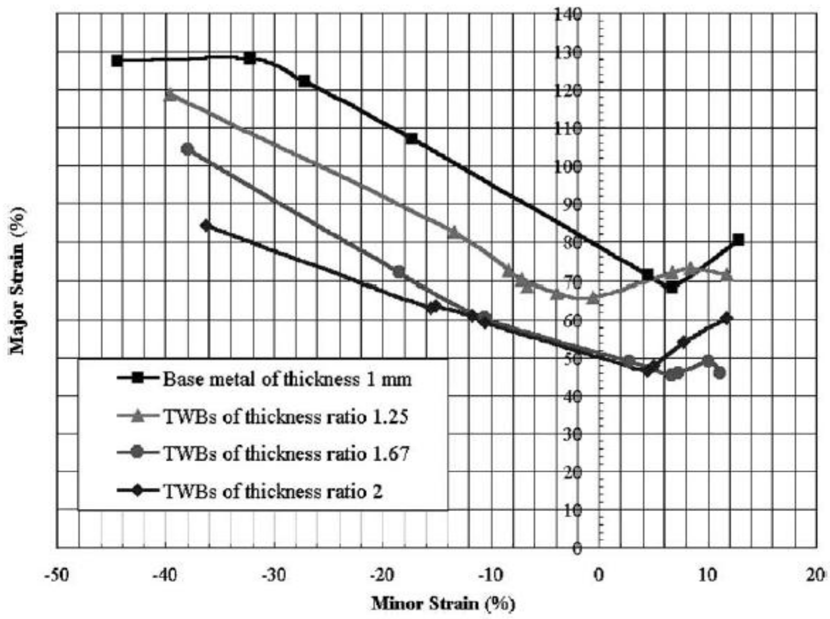

Figure 2.9: Comparing the FLDs of TWBs of different thickness ratio with the base metal of thickness 1 mm

Source: Chan *et al*. (2003)

Chan (2001) also carried out Swift bottom tests on TWBs cold rolled sheets. The TWBs had different thickness combinations of 0.7-0.8 mm, 0.7-1.0 mm and 0.8-1.0 mm, welded by an Nd:YAG laser. They used 2 mm diameter grids for measuring the major and minor strains. The weld bead was once again oriented perpendicular to the major strain axis. The forming failure was reported to occur in the thinner section of the TWB and in a direction parallel to the weld bead. However, it was reported that with the variation in width of the specimens, the distance of the failure from the weld bead also varied. With the increase in the width, the failure was observed to be closer to the weld bead. They also observed that as the thickness ratio of the TWBs increased, the LDH to failure decreased.

Ghoo (2001) has introduced a new concept of forming limit diagram for TWBs in which they carried out hemispherical dome tests on different widths of similar (0.8-0.8 mm) and dissimilar thickness (0.8-1.5 mm) TWBs. The weld bead was at the centre of the punch face and oriented parallel to the major strain direction. With the use of square grids, they measured the strains in the weld zone by generating a failure perpendicular to the weld bead. It was observed that the FLD of the weld zone in both similar and dissimilar thickness TWBs was lower than the FLD of the base metal. The deformation concentrated on a region generating higher stress while the other region may not at the same time yield any plastic deformation. As a result, the total elongation of the TWBs was much lower than the base metal.

A study done by Chan (2003), said that minimum major strain was a good measure for comparing the formability of TWBs of different thickness ratios. There was an inversely proportional relationship between thickness ratio and minimum major strain. TWBs of a thickness ratio closer to one were found to have a closer minimum major strain to those of the base metals. Microstructural study and microhardness measurement were carried out on the TWBs. The microstructural analysis showed a larger difference of grain size at the heat affected zone (HAZ) for a TWB of a higher thickness ratio. The grain size in the thinner region was larger than that in the thicker region in which it is because of the thermal cycle effects on the TWBs with different thickness ratio. During welding, both parts of the TWBs normally be attacked by the same heat source. The thinner part should have a longer recrystallization time than the thicker region during cooling. Microhardness measurement was carried out at the weld bead and across the base metals. The findings of the test indicated that the fusion zone was harder than the base metal by 60 %, while the hardness of the HAZ of TWBs of different thickness ratios could be either harder or softer than the base metal.

2.5.2 Summary

From the research, we found that the smaller the thickness combination differences between the two parts of a TWB, the higher the formability. So, we can say that in a TWB combination, both similar and dissimilar in thickness will have failure in weldment depending on the ratio.

2.5.3 Loading Direction

Shi (1993) found that the weld bead usually undergoes uni-directional deformation along the welding line and hence the positioning of the weld in the sheet blank should be carefully selected. The suggested optimum position is to place the weld perpendicular to the major strain direction. Kridli (2000) concluded that formability for the aluminum TWBs is affected by weld orientation due to the weld failure caused by the weaker properties of weld metal. Several researches (Kleemola and Kumpulainen 1980; Kusuda *et al*., 1997; Ghoo *et al*., 1998) performed LDH tests on aluminum TWBs with three different weld line orientations in 0 ^{o}, 45 ^{o} and 90 ^{o} to the loading direction. Higher LDH values can be obtained at 0 ^{o} specimens with weld failure, while LDH values decreasing at 45 ^{o} and 90 ^{o} specimens with base metal failure.

As illustrated in Figure 2.10, whenever a TWB is stretched in a major loading direction perpendicular to the weld line orientation, split can be usually be found in the thinner base metal. The thinner base metal in a TWB provides the minimum strength to resist the loading because the deformation concentrates in the thinner part that leads the failure generation. As in the parallel weld line orientation, failure usually initiates at the aluminum alloy TWB due to the low ductility of welded material (Baysore *et al*., 1995).

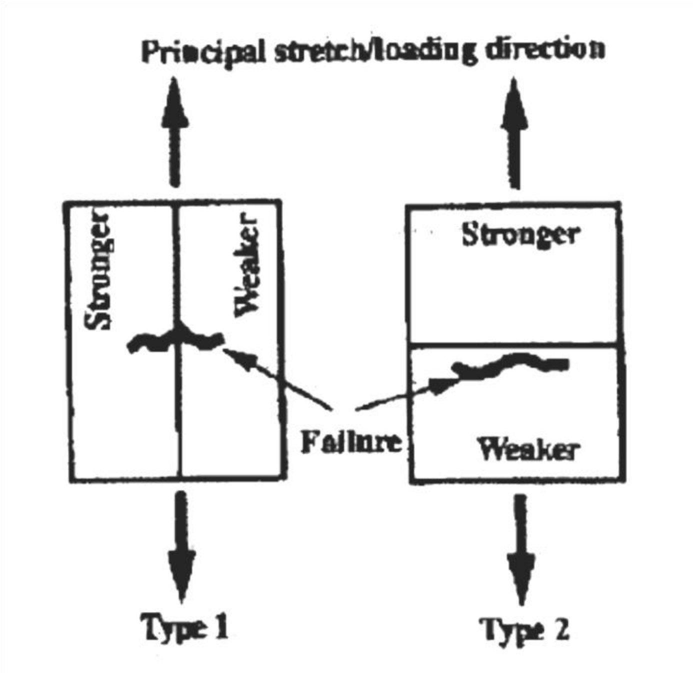

Figure 2.10: Failure mode of TWBs

Source: Saunders and Wagoner (1996)

2.5.4 Summary

Ahmetoglu *et al*. (1995), reported that the orientation of the weld line can be controlled during the process by adjusting the blank holding force in location. Also, the thinner side of TWB can be reduced by controlling the position of the weld line. From the research, we can found that most specimens at 0 ^{o} loading orientation will have failure under constant deformation.

2.6 FATIGUE OF TAILORED WELDED BLANKS

Anand (2004) has stated that for a combination of TWB, there are several factors that affect the fatigue life includes the layout of forming tool, the forces applied, and surface properties like roughness and coatings. Besides, the residual stresses, stress concentration and the strain have effect in determining the fatigue life of the combination. Fatigue failures usually occur at local areas of high stress concentration due to the abrupt change when subjected to a cyclic loading. A fatigue failure is recognized from the appearance of the fracture surface, which has a smooth region due to the rubbing action as the crack propagates and a rough region where the material fails in a ductile manner.

Wang and Ewing (1991) have compared the fatigue strength of laser welds with that of resistance spot welds of similar thickness (0.76 mm) bare SAE 1008 grade of steel. The laser welds were oriented in a direction both parallel and perpendicular to the loading direction. The fatigue strength of the laser welded blank that was oriented perpendicular to the loading direction gave the highest fatigue resistance as shown in Figure 2.11. This was mainly attributed to the high stress intensity introduced at the circumference of the spot weld due to its geometry.

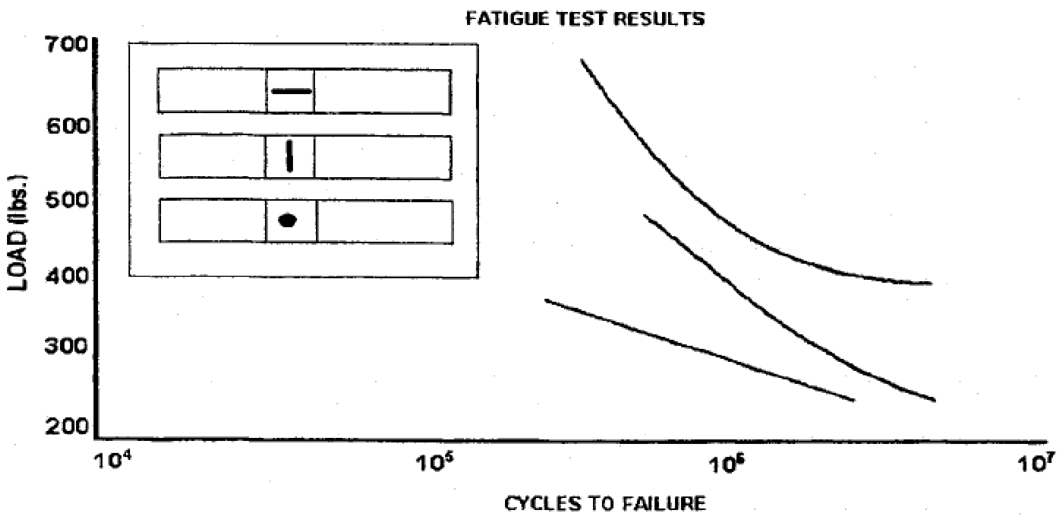

Figure 2.11: Fatigue test results for laser and spot weld

Source: Anand (2004)

Lazzarin (1995), while evaluating different welding processes, determine the fatigue strengths of dissimilar thickness (1.5 mm) laser welded sheets in both bare and hot dip galvanized conditions. The weld bead was oriented perpendicular to the loading direction. They concluded that the fatigue strength of the bare TWB was 1.4 times higher than that of the galvanized TWBs. This is because the fatigue properties are dependent on the surface condition of the material tested. Rhee (2002) evaluated the fatigue behavior of similar (0.9 mm) and dissimilar (0.9-2.0 mm) thickness laser welded sheets of bare cold rolled steel (0.016 % carbon). The weld bead was oriented both parallel and perpendicular to the loading direction. Both similar and dissimilar thickness specimens with weld bead being perpendicular to the loading direction showed similar fatigue strengths. The fatigue crack initiated in the base metal and the final fracture also occurred in the base metal.

Oh (2000) reported lower fatigue strengths for dissimilar thickness sheets in their work on similar (0.9 mm) and dissimilar (0.9-2.0 mm) thickness laser welded sheets with weld oriented both parallel and perpendicular to the loading direction. This was attributed to the stress concentration induced by the discontinuous face. Lee (1996) evaluated the fatigue strengths for dissimilar thickness (0.7-1.6 mm) TWB. They compared the laser welding process with the mash seam welding process and found that laser welded blanks achieved a higher stress level. The mash seam welds had a greater notch effect and thus lower fatigue strength. Aristotile and Fersini (1999) evaluated the fatigue strength of a production part that was formed out of a laser welded blank. The fracture was found to occur at locations having clamping holes away from the weld bead.

2.6.1 Summary

In many types of service applications metal parts subjected to repetitive or cyclic stresses will fail due to fatigue loading at a much lower stress than that which the part can withstand under the application of a single static stress. The fatigue strength of a metal or alloy is affected by factors other than the chemical composition of the metal itself. Some of the most important of these are stress concentration, surface roughness, surface condition and environment. Surface defects such as notches reduce the fatigue strength of a part. So, in the study we are going to design the specimen that are less likely having such stress raisers. In general, the smoother the surface finishes on the metal sample, the higher the fatigue strength. Rough surface create stress raisers that facilitate fatigue crack formation. Roughness is typically considered to be the high frequency and friction coefficients. So, the weld part should be in smooth surface as possible. Most fatigue failures originate at the metal surface, thus any major change in the surface condition will affect the fatigue strength of the metal as well as welded part. Also, we should consider the surrounding environment during welding since the chemical attack can accelerate the rate at which fatigue cracks propagate.

CHAPTER 3

METHODOLOGY

3.1 INTRODUCTION

In this chapter, the procedure of the study and the method used was discussed. In order to investigate the effect of thickness ratio and loading direction on the TWB, the fatigue properties of the weld specimen must be obtained. Medium carbon steels were used as the material tested. TIG welding was chose due to its advantages compare to the other type of joining method. The fatigue strength in this study was obtained from the experimental results which including test bench based on the fatigue and tensile test. Characterization test was carried out by using optical microscope and SEM to analyze the microstructure change of the weldment. The procedures of the study were briefly explained into the flow chart schematic diagram as shown in the Figure 3.1.

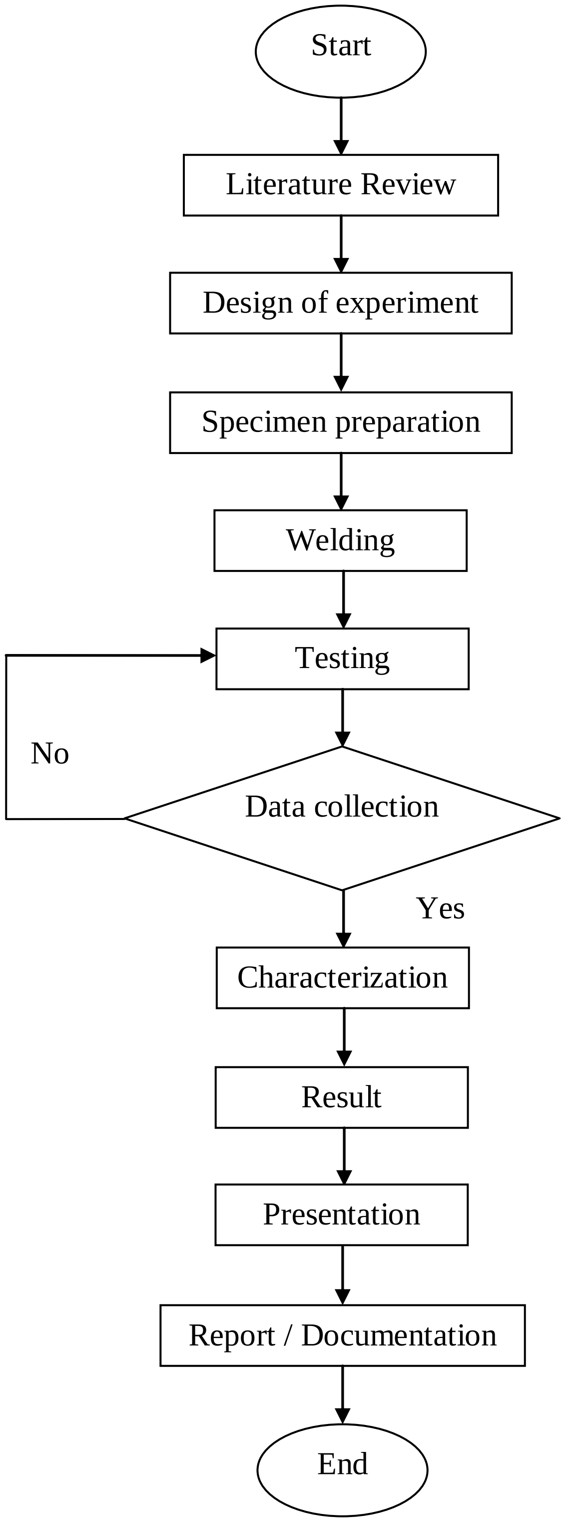

Figure 3.1: Project flow chart

3.2 FLOW CHART DESCRIPTION

3.2.1 Literature Review

The project was started with literature review and research about the title. It consist of a review on TWB background, welding processes, material properties, formability of TWB, and fatigue test of TWB. These tasks have been done through research on the internet, reference books, journals, articles and other resources.

3.2.2 Design of Experiment

In order to gather some ideas for the preliminary design of experiment, a discussion was held with supervisor. Throughout the discussion, the project objectives, scopes and background study were verified. The design of experiment was including the determination of material, machine and method of analysis.

3.2.3 Specimen Preparation

After finished with the design of experiment, we moved to specimen preparation process where the materials were obtained from the laboratory store. The material chose for the project was mild steel. The type of mild steel was AISI 1045 medium carbon steel which composition was presented in Table 3.1. It was provided in the form of around rod of 20 mm diameter. It is generally available in round rod, square bas and rectangular bar. It has a good combination of all of the typical traits of steel strength, ductility, and comparative ease of machining. Since there were two different test analyses, two different shape of material were used which were the rectangular flat and round bar shape mild steel. For the flat material, the raw material was cut by using the hydraulic shearing machine. Then, the specimen materials were cut into specified shape according to the standards ASTM E8 by using the electrode discharge machine (EDM) wire cut. While for the round bar material, the raw material was roughly cut by using the bend saw machine. Then, the specimen materials were also cut into specified shape by using the conventional lathe machine.

Table 3.1: Composition of 1045 medium carbon steel

AISI 1045 Medium Carbon Steel		
Chemical composition	Carbon, C	0.420 – 0.500 %
	Iron, Fe	98.51 – 98.98 %
	Manganese, Mn	0.60 – 0.90 %
	Phosphorus, P	0.040 %
	Sulphur, S	0.050 %
Mechanical properties	Ultimate tensile strength	565 MPa
	Yield tensile strength	310 MPa
	Elongation	16.0 %
	Vickers hardness	170

Source: The Azo Journal of Materials Online (2013)

The machining process to make a flat specimen was done using the wire cut machine as shown in the Figure 3.2. During the machine operation, the technician guided with the proper procedures to handle the machine Altogether 15 sheets of steel plates with 2 mm in thickness were clamped on the platform. The cutting speed was applied and it took almost 10 hours to complete. Then, the process was continued with the cutting of sheet plates 3 mm in thickness. The drawing schematic was shown in the in Appendix A1. Figure 3.3 show the finished specimen after the machining process was done.

Figure 3.2: General view of a Sodick AQ535L Wire Cut Machine, showing various components

Figure 3.3: Finished machining of tensile specimen

The machining process required to make the round bar specimens were turning process based on the standards ASTM E467. The parameters required to be control in the turning process were the spindle speed, feed rate and depth of cut. The spindle speed can be calculated by using the equation below:

$$N = \frac{CS \times 1000}{\pi \times d} \tag{3.1}$$

Where:

N = spindle speed (rpm)

CS = cutting speed (m/min)

d = work piece diameter (mm)

The feed rate calculation equation was as below:

$$v_f = f \text{ x } N \tag{3.2}$$

Where:

f = feed (mm/rev)

N = spindle feed (rpm)

Sample calculation for spindle speed by using the equation 3.1:

Recommendation cutting speed = 60-135 m/min

Diameter of work piece = 20 mm

$$N = \frac{60 \times 1000}{\pi \times 20}$$
$$= 955 \text{ rpm}$$

Sample calculation for feed rate by using the equation 3.2:

Recommendation feed = 0.15-1.1 mm/rev

Spindle speed = 1600 rpm

$$\begin{aligned} v_f &= f \text{ x } N \\ &= 0.15 \text{ x } 1600 \\ &= 240 \text{ mm/min} \end{aligned}$$

Refer to Appendix A4 for general recommendation for turning operation. Table 3.2 was listed the parameters used for turning operation. The turning process to make the round bar specimen was by using the conventional lathe machine as shown in the Figure 3.4. Figure 3.5 showed the raw specimen before turning process while Figure 3.7 showed the finished specimen after the turning. In Figure 3.6, the specimen was undergone the turning operation.

Table 3.2: Parameters for turning operation

Parameters	Value
Spindle speed (rpm)	1600
Feed (mm/rev)	0.15
Feed rate (mm/min)	240
Depth of cut (mm)	0.2

The step to use the conventional lathe machine was as below:

1. The lathe machine was set up to be ready to perform the process.
2. The lathe machine was switched on to make sure the power supply was applied.
3. The cutting tool was set up. The cutting tool used was the ball bearing live centre to make the center drill for each material.
4. The mild steel bar was attached to the spindle and clamped to the chucks. Make sure the mild steel bar was tightly held.
5. The cutting speed used was in the range of 60-135 m/min.
6. The work piece was then being machined according to the geometry shape in the drawing as shown in the Appendix A1.
7. The feed rate in turning was set to be 0.15 mm/rev while the depth of cut was set to be 0.2 mm.
8. After finished with the turning, the work piece was measured by using vernier caliper.
9. The process was repeated until 10 pieces of materials was done.

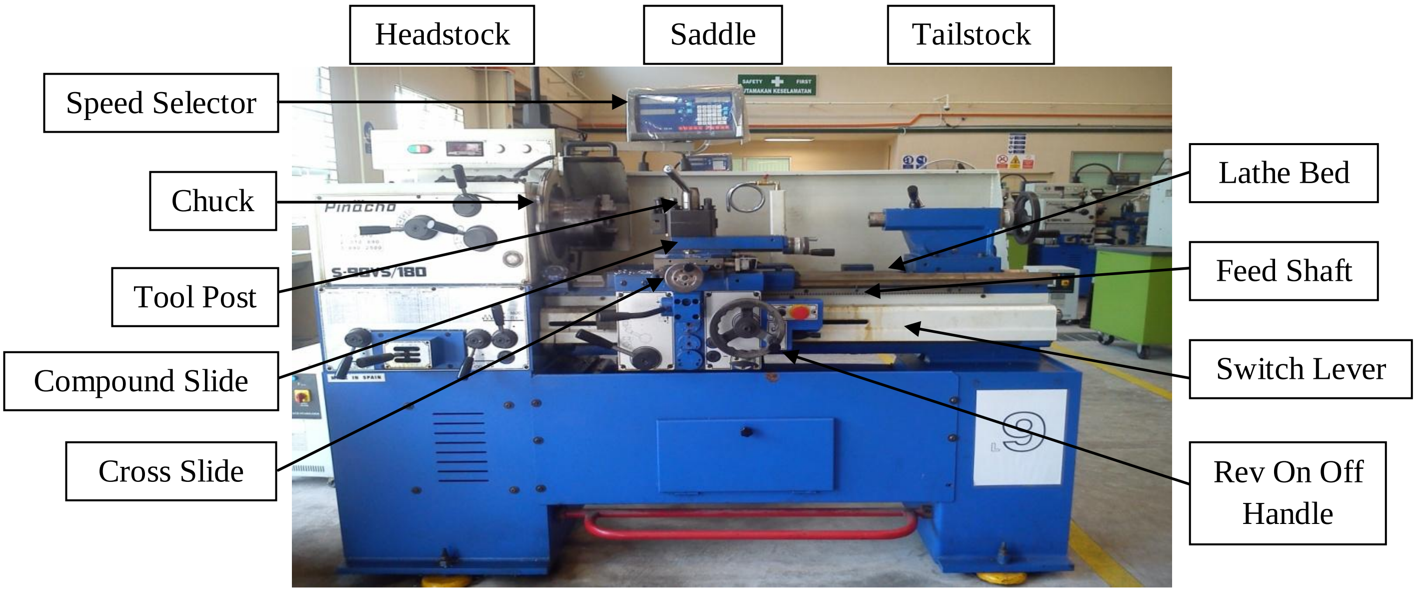

Figure 3.4: General view of a Pinacho S 90VS/180 Conventional lathe machine, showing various components

Figure 3.5: Raw materials of medium carbon steels

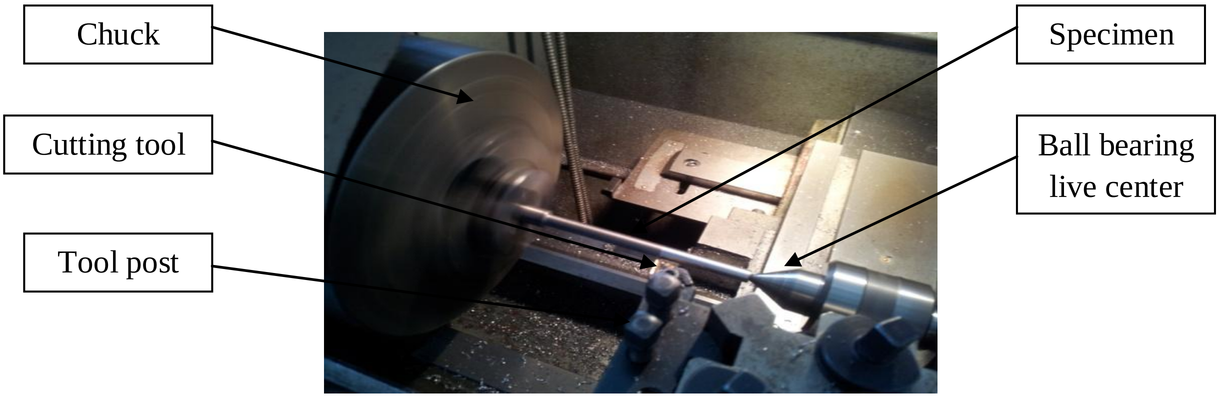

Figure 3.6: Turning process of conventional lathe machine

Figure 3.7: Finished machining fatigue specimen

3.2.4. Welding

The next process followed by the material preparation was welding. The parameters used during the welding process were described as Table 3.3. The requirement for each specimens' joining are described briefly in Table 3.4 and Figure 3.8. The TIG welding machine that was used throughout the welding works can be seen in Figure 3.9.

Table 3.3: TIG welding parameters

Parameters	Value
Current	Direct current
Current speed (A)	45 A
Voltage (V)	13 V
Filler	ER 70 S
Tungsten electrode	Thoriated ThO_2

Table 3.4: Welding specifications

Thickness	Specimen	Loading Direction
2 mm – 2 mm	1	90^{o}
	2	45^{o}
3 mm – 3 mm	3	90^{o}
	4	45^{o}
2 mm – 3 mm	5	90^{o}
	6	45^{o}

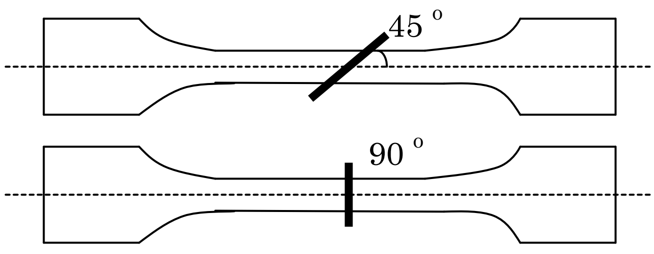

Figure 3.8: Tensile test welding specifications

Figure 3.9: A Syncrowave 200 Miller TIG welding machine

The welding types that we used for the project was TIG welding. The method of joining two or more parts into an assembled entity is commonly known as TWB. TIG welding is parts of arc welding group that refers to a group of welding processes in which heating of the metals is accomplished by an electric arc as shown in Figure 3.10. Also, arc welding is included in the fusion welding where the process used heat to melt the base metals. During the operation, a filler metal was added to the molten pool to facilitate the process. Thus, bulk and strength was provided to the welded joint. Tungsten was used as it had a good electrode material due to its high melting point.

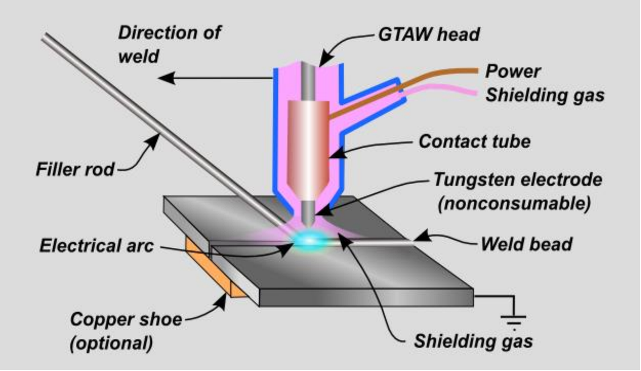

Figure 3.10: Cross section view during TIG welding

Source: Vince (2013)

Welding produces a solid connection between the two pieces called a weld joint as shown in the Figure 3.11. A weld joint is the junction of the edges or surfaces of parts that have been joined by welding. The project used the basic type of joint that was butt joint. In this joint type, the parts were laid in the same plane and joined at their edges as seen in Figure 3.12. Both flat and round bar specimens were welded to form the tailored welded blanks as shown in Figure 3.13. Later, the TWB specimen is inspected to check the quality of the welded joint. The welding inspection method used is visual inspection to examine the weldment. The weldment is visually examined for warping, cracks, cavities, incomplete fusion and other visible defects. However, the visual inspection is limited only that surface defects are detectable, visual method cannot discovered the internal defects.

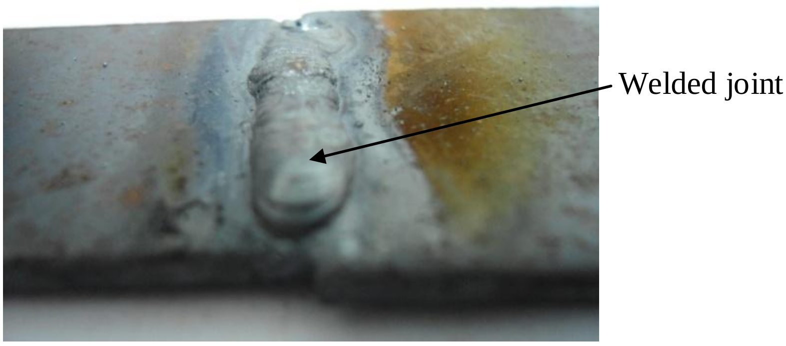

Figure 3.11: The completed end view weldment

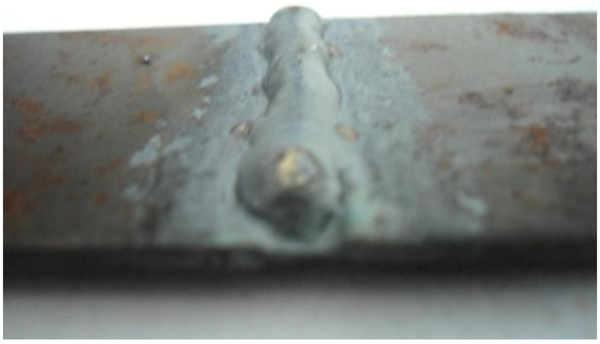

Figure 3.12: Butt joint TWBs combination

(a) (b)

Figure 3.13: Welded specimen for (a) tensile specimen and (b) fatigue specimen

3.2.5 Testing

After finished with the welding, we carried on the study with specimens testing. There were two tests that had been done which were tensile test and fatigue test.

A. Tensile test

The tensile is used to evaluate the strength of metals. By definition, engineering stress, σ is equal to the average uniaxial tensile force, F divided by the original cross-sectional area A_o.

$$\text{Engineering stress, } \sigma \text{ (N/m}^2\text{)} = \frac{\text{average uniaxial tensile force,F}}{\text{original cross−sectional area,}A_o} \qquad (4.1)$$

While engineering strain, ϵ which is caused by the action of a uniaxial tensile force on a specimen, is the ratio of the change in length of the specimen in the direction of the force divided by the original length of specimen required.

$$\text{Engineering strain, } \epsilon \text{ (m/m)} = \frac{\text{change in length of specimen,}\Delta l}{\text{original length of specimen,}l_o} \qquad (4.2)$$

In this test, a metal specimen is pulled to failure in a relatively short time at a constant rate. The force on the specimen being tested is measured by the load cell while the strain is obtained from the extensometer attached to the specimen and the data is collected in a computer control software package. The force data obtained is then converted to engineering stress data and a plot of engineering stress versus engineering strain is constructed.

The mechanical properties of the specimens obtained from the engineering tensile test are yield strength, ultimate tensile strength, breaking strength and elastic or Young's modulus of the material. The yield strength is the strength at which a metal or alloys shows significant plastic deformation. In this study, the yield strength is chosen when 0.2 percent plastic strain has taken place which also called the 0.2 percent offset yield strength. The 0.2 percent offset yield strength is the stress where the horizontal line intersects the stress axis. The ultimate yield strength is maximum strength reached in the engineering stress-strain curve. The modulus elasticity is related to the bounding strength between the atoms in a metal or alloy. Linear relationship between stress and strain in the elastic region of the engineering stress-strain diagram is described by Hooke's law.

$$\text{Modulus of elasticity, E (Pa)} = \frac{\text{stress}, \sigma}{\text{strain}, \epsilon} \tag{4.3}$$

The tensile test was conducted by using Instron Universal Tensile Testing Machine Model 3369 as shown in Figure 3.14. In this test, the specimen was pulled to failure in a relatively short time at a constant rate. The force on the specimen being tested was measured by the load cell while the strain was obtained from the extensometer attached to the specimen and the data was collected in a computer control software package. From the data obtained, we computed all the stress strain values and came out with a resulting curve called the stress-strain diagram. The yield strength, ultimate tensile strength, breaking strength and elastic or Young's modulus of the material was determined from this curve.

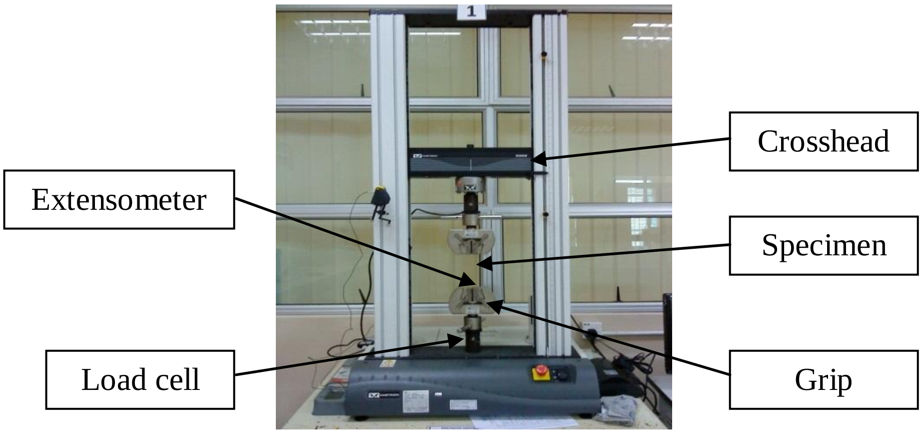

Figure 3.14: General view of an Instron Universal Tensile Testing Machine Model 3369, showing various components

The machine was setup according to standard procedure published by the manufacturer and the following were the design of the experiment.

a. Test preparations

- The length, width and thickness of the gage of the specimens were specified, measured as shown in the Appendix.
- The cross head speed applied during this test was 1 mm/min.

b. Experiment procedures

1. The “IX series” icon on the computer was double clicked.
2. The specimen was loaded into the lower and upper grip. Make sure the specimen was straight.
3. “Method” icon was clicked. The specimen parameter and crosshead speed were set.
4. “Test” icon was clicked and sample file name was entering followed by the operator’s name.
5. A test method was chose according to the application such as tensile.
6. The load and strain were reset.
7. “Start Test” icon was clicked.

8. When the test finished, the result of the experiment was viewed by click to the utilities in the main screen.
9. The stress-strain diagram was plotted as soon as each specimen was tested.

B. Fatigue test

The fatigue test was conducted by using the rotating bending fatigue machine as shown in Figure 3.15. Data from this test were plotted in the form of SN curves in which the stress S to cause failure was plotted against the number of cycles N at which failure occurs.

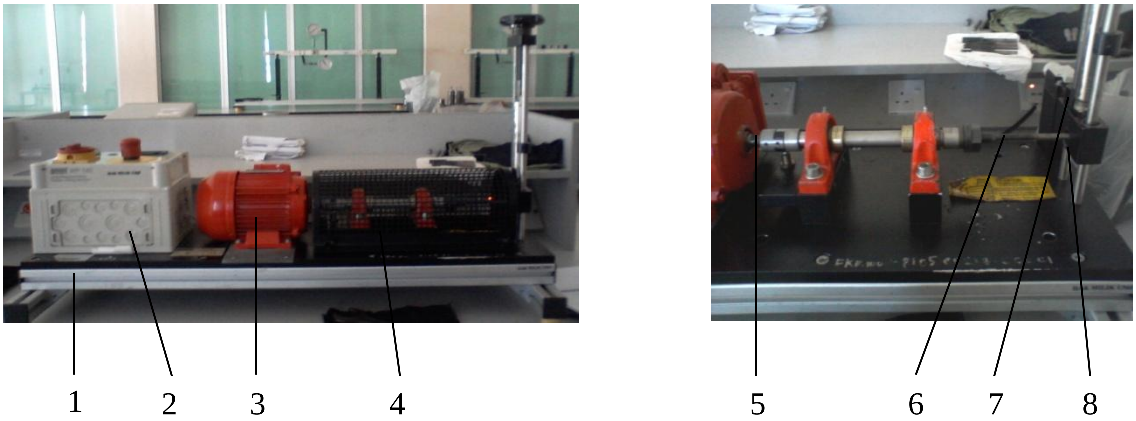

1 – Base frame
2 – Switch box
3 – Drive motor
4 – Protective hood

5 – Speed sensor
6 – Specimen
7 – Load gauge
8 – Load bearing

Figure 3.15: General view of a WP 140 Fatigue Testing Apparatus, showing various components

a. Experiment setup

The machine is commissioned and test run to ensure that it is in ready for operation condition. Firstly, the revolving fatigue testing machine was erected and connected to the power supply. Secondly, the protective hook was removed (unhook the fasteners by rotating the knobs to the left). Thirdly, the load device was relieved using the hand wheel (move the load bearing down to the bottom). Fourthly, any sample which may be in position was removed and the union nut was lightly tightened on the chuck. Finally, the protective hood was mounted and locked with all four knobs. Please do ensure that the following things were properly checked:

i. Emergency off switch was released (pulled out).
ii. The machine was switched on using the master switch.
iii. The counter was reset using the RST button and counter must display zero.
iv. The motor was started up using the motor control switch.
v. The spindle was checked so that it was running smoothly and true.
vi. The counter was checked so that it was counting correctly.
vii. The automatic stop device was checked so that it is functioning.

b. Test preparation

- The length, width and thickness of the gage of the specimens were specified, measured and shown in Appendix A1.

c. Experiment procedures

1. The experiment was started with the non-weld mild steel to study the maximum load to rupture.
2. The experiment was repeated by reducing the load generally from one specimen to the next from the maximum value F= 250 N.
3. The numbers of load cycles were determined until the specimen ruptures.
4. The stress-number diagram was plotted and fatigue limit of the specimen was determined.

3.2.6 Characterization

After tensile and fatigue test, characterization analysis was conducted. There are two analyses which were carried out using SEM and inverted microscope. Both analyses had the same procedure of preparation before the test. The process to prepare the mounting was as followed:

1. The fatigue and tensile sample were cross sectioned by using cutoff wheel.
2. The surface of the automatic mounting press was applied with a release agent liquid known as epoxide. The readily sectioned part was put on the hot plate and an amount of bakelite was poured into the mounting mould.
3. The automatic mounting press machine was switched on with the parameter of pressure was 290 bar, heated and preheated for 1 min before it was cooled in 3 min.
4. The mounted samples were grinded by using roll grinder. The steps to grind the sample were shown in Table 3.5.

Table 3.5: Parameters used for surface grinding stage

Size grit	Time (s)	Wheel speed (rpm)	Pressure (psi)
180	120	300	32
320	60	300	32
400	60	300	32
600	60	300	32

5. The samples then were polished by using roll polisher. The steps to polish the sample were shown in Table 3.6.

Table 3.6: Parameters used for surface polishing stage

	Time (s)	Wheel speed (rpm)	Pressure (psi)
Microd extender	300	250	25
0.05 micron colloidal silica	120	150	15

6. The samples were etched for 3 seconds before the test analysis.

A. Microstructure test

After the sample preparation, characterization test was conducted. There are various instruments used to study and understand the behavior of materials based on their microstructures, existing defects, microconstituents, and other features and characteristics specific to the internal structure. In the project, inverted microscope and SEM were used to investigate the internal and surface features of materials.

An inverted microscope is a microscope structured with its light source and condenser on the top, above the stage pointing down, while the objectives and turret are below the stage pointing up as shown in Figure 3.17. It is useful for observing grain size, grain boundary, existence of various phases, internal damage, and some defects where the polished samples are placed on top of the stage and viewed from underneath using reflecting objectives. Figure 3.16 below designates the main components of the IM7000 Series Inverted Metallurgical Microscope.

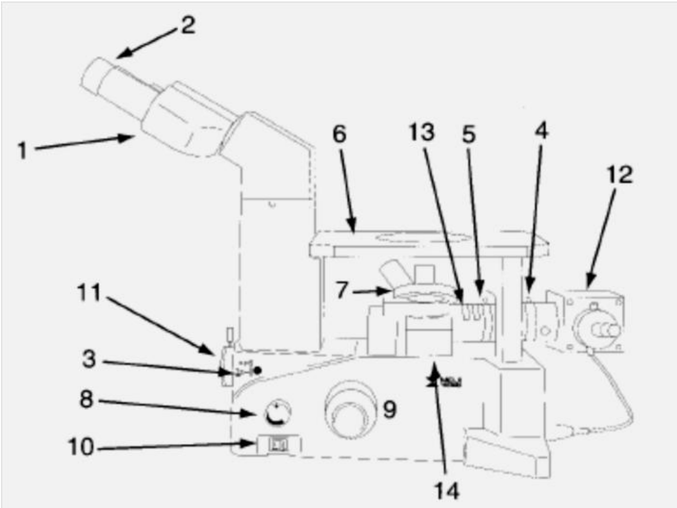

1 Binocular head, 30^{o} inclination

2 Eyepieces, SWH10X (15X & 20X optional)

3 Beamsplitter for front camera port

4 Aperture diaphragm

5 Field iris diaphragm

6 Specimen stage

7 Quintuple nosepiece & brightfield objectives

8 Low positioned variable brightness control

9 Coaxial coarse and fine focusing controls

10 Power switch

11 Front camera port

12 Integrated illuminator 6V 30W

13 Filter slots (2)

14 Slide in semi rotatable analyzer

Figure 3.16: Components of inverted microscope

Figure 3.17: IM7000 Series Inverted Microscope

B. Fracture test

SEM is a tool used for microscopic feature measurement, fracture characterization, microstructure studies, thin coating evaluations, surface contamination examination, and failure analysis of materials. The diagram is shown in Figure 3.18. SEM impinges a beam of electrons in a pinpointed spot on the surface of a target specimen and collects it. Then, it displays the electronic signals given off by the target material. The principles of operation are basically as followed. An electron gun produces an electron beam in an evacuated column that is focused and directed so that it impinges on a small spot on the target. Scanning coils allow the beam to scan a small area of the surface of the sample. Low-angle backscattered electrons interact with the protuberances of the surface and generate secondary backscattered electrons to produce an electronic signal. Secondary electrons are electrons that are ejected from the target metal atoms after being struck by primary electrons from the electron beam. The secondary electron later produces an image having a depth of field of up to about 300 times compare to the optical microscope. The resolution of many SEM instruments is about 5 nm, with a wide range of magnification.

SEM is particularly useful in materials analysis for the examination of fracture surfaces of metals. SEM are used to determine whether a fractured surface is intergranular (along the grain boundary), transgranular (across the grain), or a mixture of both. The samples to be analyzed using standard SEM are often coated with gold or other heavy metals to achieve better resolution and signal quality.

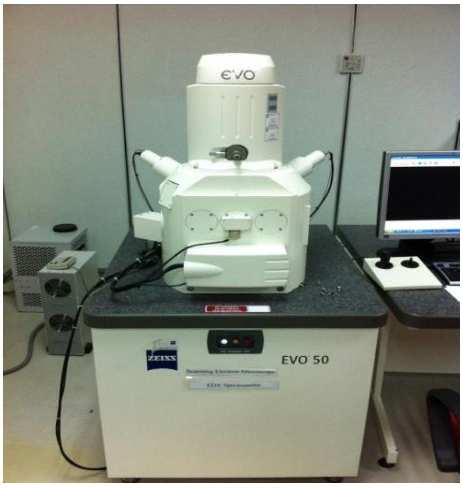

Figure 3.18: Scanning Electron Microscopy EVO®50 02-73

The steps involved in SEM sample preparation are likely same as the preparation for the microstructure test which include sectioning, mounting, grinding, polishing and etching. Each of these steps are crucial and will affect the outcome of the test, thus it has to be performed in perfection. After all the steps have been performed, the mounted sample was ready to be viewed.

3.2.7 Preliminary Result

After all the experiment has conducted, the data result was collected. The preliminary results were the stress-strain and stress-number (S-N curve) diagram as shown in Figure 3.19 and Figure 3.20 respectively.

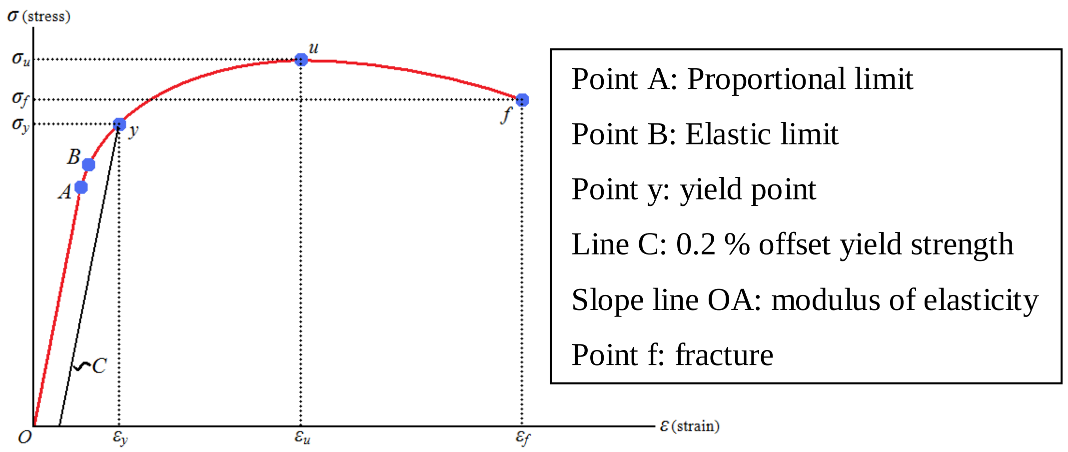

Figure 3.19: Stress strain diagram

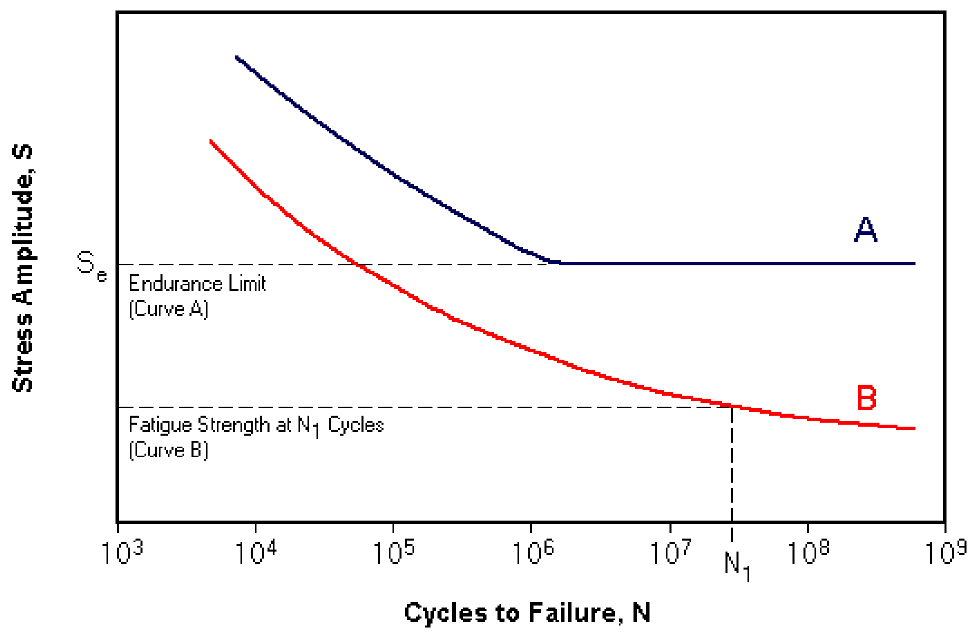

Figure 3.20: SN curve diagram

3.2.8 Presentation and Documentation

Lastly, the final report writing was prepared together with presentation session. The first presentation was held at the end of the first semester while the second presentation will be held at week 15 of the second semester. The first presentation outline includes 3 chapters which are introduction, literature review and methodology on the study. Chapter 1 reviewed on the problem statement, objectives, scopes and background of the study. While for the second presentation, the result and study outcomes were shown. The result and test analysis obtained were discussed. Later, the report writing was done according to the FKM thesis format guided. The task scheduled took fourteen weeks to completely done.

3.2.9 Gantt Chart

Gantt chart is a planning schedule for a project that ensures the progresses are on the track. The detail of the Gantt chart for this study was shown in Appendix A5 and A6.

CHAPTER 4

RESULTS AND DISCUSSION

4.1 INTRODUCTION

The analysis methods used in the current study were the rotating bending fatigue testing and tensile testing. Fatigue test was conducted to define the life cycle of fatigue before it fail due to fatigue loading. The purpose of the experiment was to determine the fatigue life of a TWB. In addition, tensile test was conducted to evaluate the strength of a TWB depending of the material's characteristics.

4.2 MATERIAL COMPOSITION

The material composition for the specimens has been analyzed by using spectrometer foundry machine. The main purpose for this analysis was to define the percent of chemical composition in the material that we used for the current study. The percentage of the chemical composition for the material was shown in Table 4.1 and for more detail results can be found in Appendix A2. The composition of carbon in the material used was about 0.4 % and this showed that the material is a medium carbon steel.

Table 4.1: Chemical composition of the material

Chemical Composition	Reading							
	1	**2**	**3**	**4**	**5**	**6**	**7**	**Average (%)**
Iron (Fe)	95.2	95.2	95.4	96.3	95.6	96.0	96.6	95.8
Carbon (C)	0.142	0.486	0.548	0.439	0.520	0.390	0.505	0.471
Silicon (Si)	0.328	0.505	0.569	0.344	0.579	0.514	0.336	0.454
Manganese (Mn)	0.662	1.12	1,19	0.985	1.29	1.18	1.23	1.09
Phosphorus (P)	0.327	0.162	0.103	0.112	0.1	0.087	0.075	0.138
Sulphur (S)	0.150	0.150	0.150	0.150	0.150	0.150	0.150	0.150
Chromium (Cr)	0.178	0.239	0.240	0.209	0.314	0.289	0.227	0.242
Molybdenum (Mo)	0.087	0.063	0.052	0.045	0.069	0.064	0.035	0.059
Nickel (Ni)	0.484	0.450	0.385	0.323	0.329	0.313	0.228	0.359
Aluminum (Al)	0.041	0.048	0.045	0.034	0.037	0.034	0.041	0.040

4.3 WELD QUALITY

The TWB specimen is inspected to check the quality of the welded joint. The welding inspection method used is visual inspection to examine the weldment.Defects that occur in welding during the study can be seen in the Figure 4.1. A brief description of each defects are explained as below.

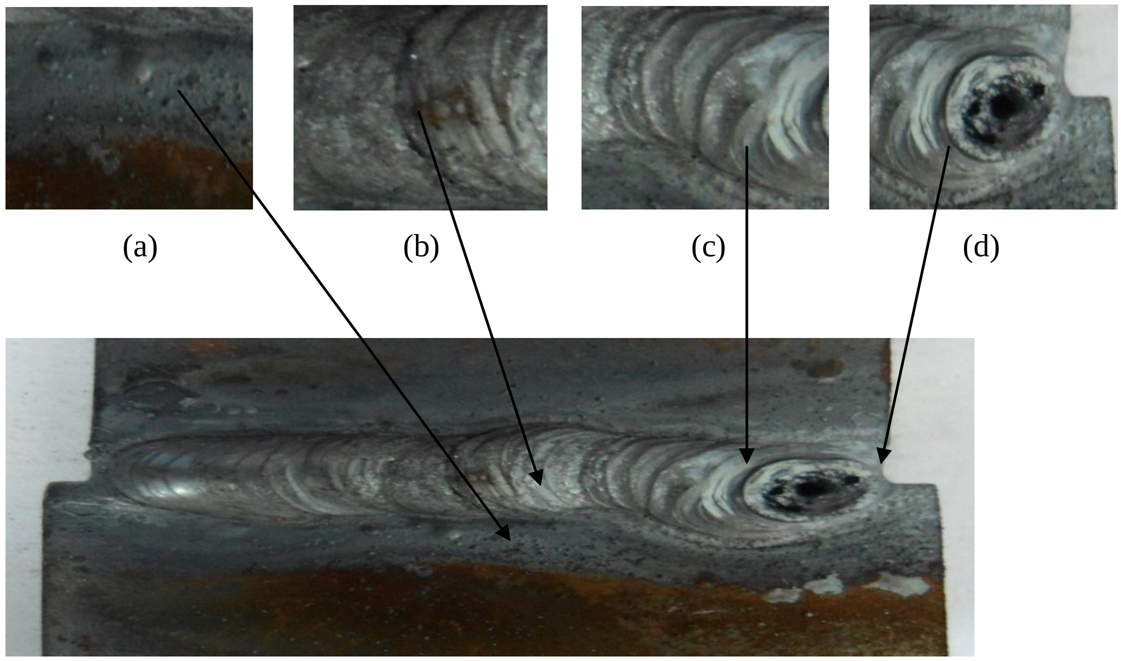

Figure 4.1: Various forms of welding defects: (a) spatters, (b) cracks, (c) incomplete fills, and (d) cavities

(a) Spatters

Excessive spatter occurred due to metal particles expelled out from the molten metal pool under the effect of harsh arc during welding. These particles are not the part of weld but freeze out in small tiny balls along the weld bead.

(b) Cracks

Cracks are fracture type interruptions occurred on the weld surface.

(c) Incomplete fills

The common cause for incomplete fill is due to not enough weld material deposited to fill the weld joint.

(d) Cavities

These kinds of defect include various porosity and shrinkage voids. Porosity consists of small voids in the weld metal formed by gases entrapped during solidification. Porosity usually results from inclusion of atmospheric gases, sulphur in the weld metal, or contaminants on the surfaces. Shrinkage voids are cavities formed by shrinkage during solidification. Also, the porosity may be due to improper shielding gas coverage, the used of wrong shielding gas of filler metal, too much heat and the base metal is not cleanly properly.

4.4 TENSILE TEST

The experiment was conducted with six different characteristics of welded specimens. The specimens are different in terms of thickness and loading direction. Figure 4.2 showed the results of tensile test. The engineering stress-strain diagram for medium carbon steel that we obtained from the tensile test can be obtained in Appendix A3. Table 4.2 summarize the data collected from the test.

(a)

(b)

(c)

(d)

(e)

(f)

Figure 4.2: Schematic of TWBs after the tensile test: (a) Same thickness, t=2 mm with 90 ^{o} orientation; (b) Same thickness, t=2 mm with 45 ^{o} orientation; (c) Same thickness, t=3 mm with 90 ^{o} orientation; (d) Same thickness, t=3 mm with 45 ^{o} orientation; (e) Different thickness, t=2 mm & 3 mm with 90 ^{o} orientation; (f) Different thickness, t=2 mm & 3 mm with 45 ^{o} orientation

Table 4.2: The tensile test data collection

Specimen	Tensile stress at yield (MPa)	Modulus (MPa)	Tensile stress at tensile strength (MPa)	Tensile stress at break (MPa)
1	292.36	22502.07	292.43	0.11
2	391.79	9851.68	491.88	143.45
3	277.36	14019.41	343.69	77.66
4	280.24	13586.29	342.45	0.25
5	328.53	12806.22	376.06	-0.09
6	411.71	12651.19	489.92	147.81

From the results obtained, each material experienced its own distinctive material properties. In a similar thickness TWB combination (2 mm-2 mm), both specimens with different loading direction, the failure occurs on the weldment. It was noticed that the maximum strength for each material is high enough to achieve the ultimate tensile strength for carbon steel. However, the ultimate tensile strength can give some indication of the presence of defects. If the weldment contains porosity or inclusions, these defects may cause the ultimate tensile strength of the welded specimen to be lower than normal. This statement was proved by the cross section on the TWB as shown in Figure 4.3. In the case of a dissimilar thickness TWB (2 mm-3 mm), failure occurred in the thinner material. In a TWB consisting of materials having different thickness with similar strength, most of the strain distributed in the thinner material as it has a lower resistance to the applied force than the thicker material and thus the failure is always associated with the thinner material. The experiment on the TWBs was conducted with two different weld line orientations in 45 ^{o} and 90 ^{o} to the loading direction. The failures resulted to occur at the weaker properties and thinner material. These findings are summarized in Table 4.3. It was found that all TWBs failure locations were similar and the failures propagated parallel to the weld bead.

Figure 4.3: Cross section on TWB after tensile test

Table 4.3: Failure location and orientation in the specimens

Specimen	Location of the fracture from the weld bead	Orientation of the fracture with respect to the weld bead
1	At the weld bead	Parallel
2	15 mm from the weld	Parallel
3	12 mm from the weld	Parallel
4	2 mm from the weld	Parallel
5	7 mm from the weld	Parallel
6	5 mm from the weld	Parallel

The stress strain curve obtained shows a great variation in ultimate tensile. The TWBs combinations of different thickness and loading direction have greatly affect the tensile strength and ductility of the weldment. As discussed previously, presence of defects can affect the strength of the metal. By referring to the Appendix, specimen 1 has low ultimate tensile strength which was 292.43 MPa. The percent elongation and reduction in area were decreased due to the porosity present in the weldment. Specimen 2 and specimen 6 show similar ultimate tensile strength where they achieved 491.44 MPa and 489.92 MPa respectively. The specimens have uniform elongation and localized necking before reached the fracture point. The transition between the elastic and plastic deformation shows a maximum followed by a sudden drop in yield stress. At the instant, the grip pulling the end of the tensile specimen undergoes a sudden acceleration. When the load drops to a lower stress, the speed of grip and the associated strain rate in the tensile specimen decelerate to lower values. The phenomena repeated in the tensile testing of specimen 3 and specimen 4. Both of the specimens produce non-homogeneous deformation in the elastic region. This might come from a contraction perpendicular to the extension by a tensile load. Also, they have low tensile strength than that other specimens, such that 343.69 MPa for specimen 3 and 342.45 MPa for specimen 4. Specimen 5 reached 376.06 MPa of ultimate tensile strength and has high toughness. The yield stress gradually increased until it reached ultimate stress point and fracture occurred.

Anand (2004) has stated that the failure occurs in the weld in a direction perpendicular to the base metal, the reason behind it is acceptable. Based on the guideline, the TWBs in the present work are all acceptable. Chan *et al.*(2003) carried out the tensile test of the TWBs with the weld being at the centre and oriented perpendicular to the loading axis. They found no significant difference in the tensile strengths of the TWBs and their relative thinner base metals. Ghoo *et al.* (2001) and Abdullah *et al.* (2001) have evaluated the mechanical properties of weldment in the steel TWBs, by using various methods like analytical equations for work-hardening and anisotropy, and rule of mixtures. They reported that the base metal has lower yield strength and higher ductility than the weld metal. Therefore in this study, the tensile properties of both thinner and thicker base metals (2 mm and 3 mm) were determined as opposed to the TWB combinations.

4.5 FATIGUE TEST

The fatigue tests were conducted in order to study the number of cycles to failure for medium carbon steel specimens. The tests were carried out according to the procedure described in Chapter 3. The recorded data for the stress amplitude and number of cycles is shown in Appendix. The obtained S-N curve for the TWB combinations was shown in Figure 4.4. S-N test data are usually displayed on a log-log plot, with the actual S-N line representing the mean of the data from the test as shown in Figure 4.5.

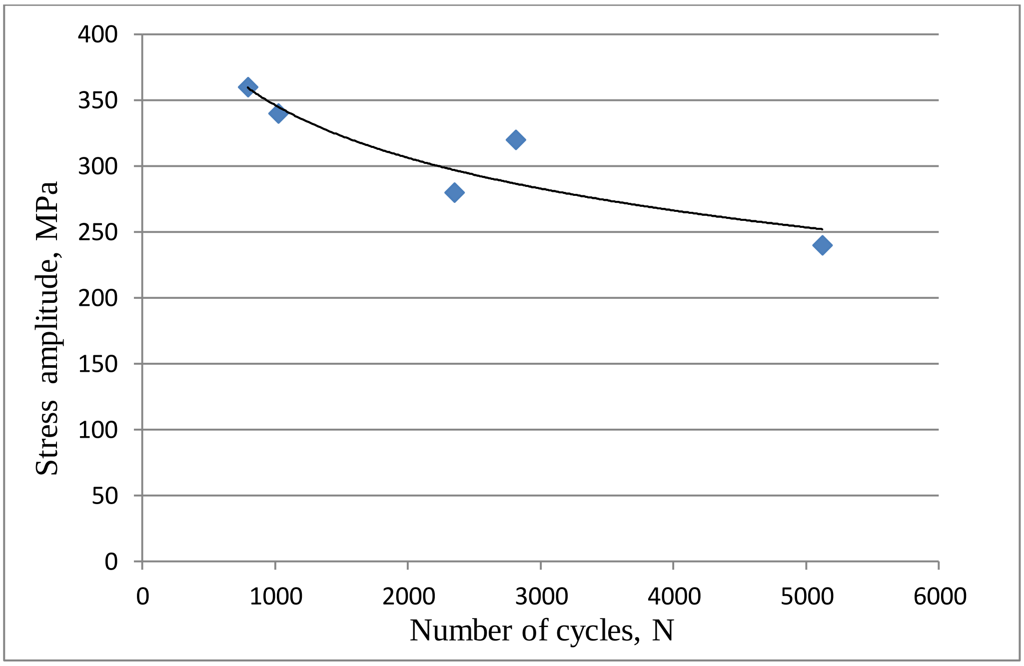

Figure 4.4: S-N curves for the TWB combinations

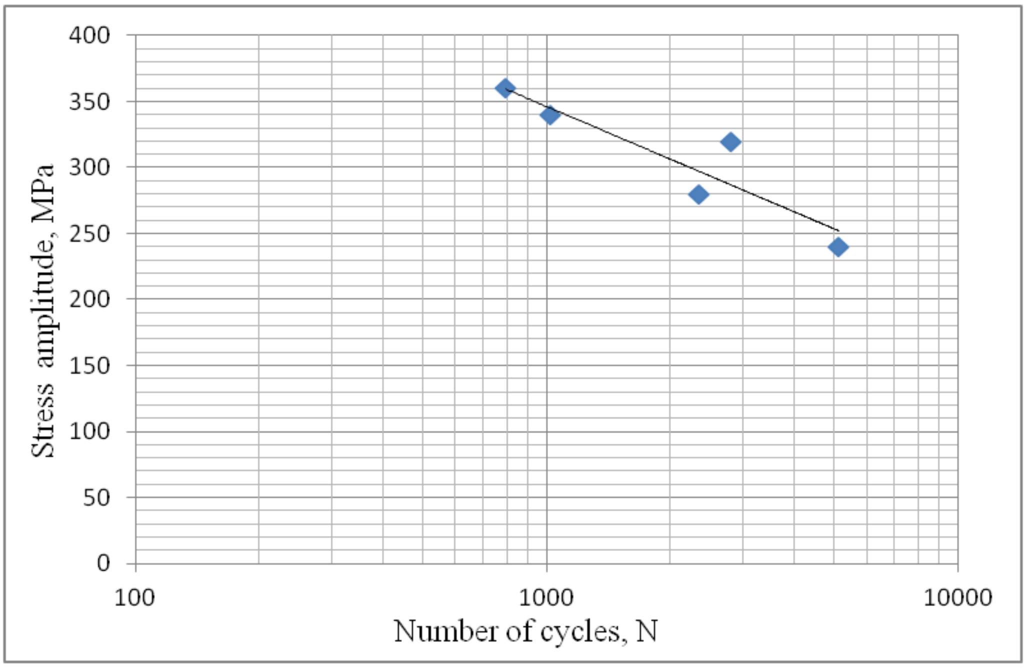

Figure 4.5: Log-log S-N curve

It was seen from Figure 4.4 that the highest fatigue limit was 360 MPa compared to the base metal with 500 MPa. The observation showed that a decrease in fatigue strength as the number of cycles was increased. Steel alloys exhibit an endurance limit that is about one-half their tensile strength. However, in the current study the materials do not exhibit well-defined endurance limit. It might due to periodic overloads that lead to the formation of microcracks, corrosive environment due to fatigue corrosion interaction and high temperature. Influences that can affect the endurance limit include surface finish, temperature, stress concentration, notch sensitivity and environment. Welding joints in TWBs combination reduce the crack initiation part of the fatigue life. Hence, the fatigue life of a material with welding is shorter than the life of base metal.

A fatigue failure usually originates at appoint of stress concentration such as a sharp corner or at a metallurgical inclusion. Once nucleated, the crack propagates across the part under the cyclic stresses. Finally, the remaining section becomes so small that it can no longer support the load and complete fracture occurs. Usually, there are two distinct types of surface areas that can be recognized. Firstly, a smooth surface region due to the rubbing action between the open surface regions as the crack propagates across the section and secondly a rough surface area formed by the fracture when the load becomes too high for remaining cross section. Figure 4.6 show sample of fatigue crack surface. When the welded structure was subjected to fatigue and impact loading, the component fatigue failures take place at the welded connections. Welding affects the material by the process of heating and subsequent subsequent cooling as well as by the fusion process with additional filler material. Furthermore, a weld is usually far from being perfect, containing inclusions, cavities, undercuts and others. The shape of the weld profile and non-welded create high stress concentrations. Residual stresses and distortions due to the welding process also did affect the fatigue behaviour.

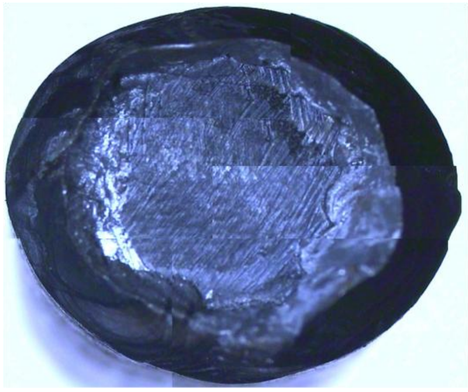

Figure 4.6: Fatigue crack surface

4.6 MICROSTRUCTURE TEST

Optical metallography techniques are used to study the features and internal makeup of materials. The surface of the specimen of the material was prepared through a detailed procedure in Chapter 3. The weld profiles were observed at 10X magnification to reveal the different zones in the specimen. The weld consist of base material, heat affected zone (HAZ) and fusion zone as shown in Figure 4.7. The microstructure of the weld cross sections were shown in Figure 4.8.

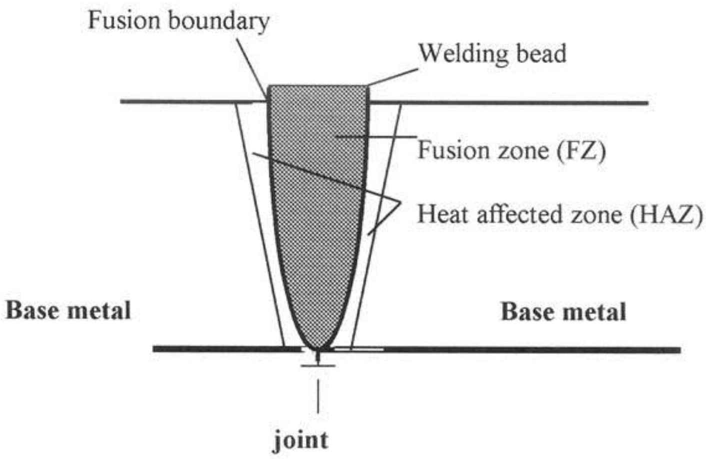

Figure 4.7: Cross section of weld joints

Microstructure examinations on the cross section of the weld were carried out. Figure show microstructure in different regions of the different thickness (2mm/3 mm) TWBs combination, such as the base metal region, the HAZ and the fusion zone. Figure 4.8 (a) show the microstructure in the base metal region mainly composed of elongated equiaxed ferrite grains. Small regions of pearlite (dark area) are present in the base metal microstructure. The microstructure in the HAZ of the weld could vary with distance from the fusion boundary. It can be divided into three major regions: the grain coarsening, grain refining and partial grain refining region. The partial grain refining region adjacent to the base metal contains very fine grain of pearlite and ferrite. Small pearlite and ferrite appear in grain refining region and this region is next to the partial grain refining region. The grain coarsening region adjacent to the weld fusion zone composes of coarsen austenite. The microstructure of the fusion zone can be observed in Figure 4.8 (b). By comparing the grain size of microstructure, Figure 4.9 show microstructure for same thickness (2 mm) TWBs combination are having similar grain size with different thickness TWBs combination.

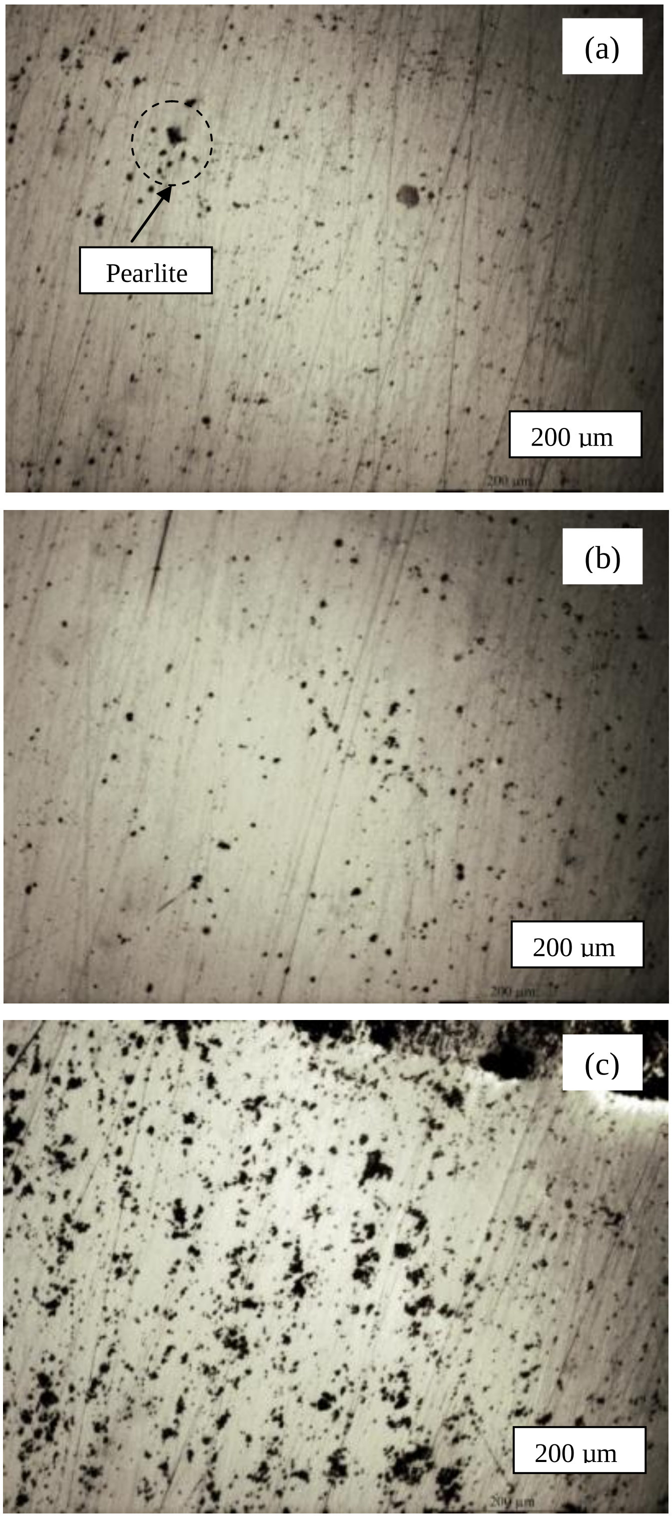

Figure 4.8: Micrographs showing the microstructure change in medium carbon steel joints before etching for different thickness of TWBs combination (a) base metal, (b) weld zone, and (c) HAZ

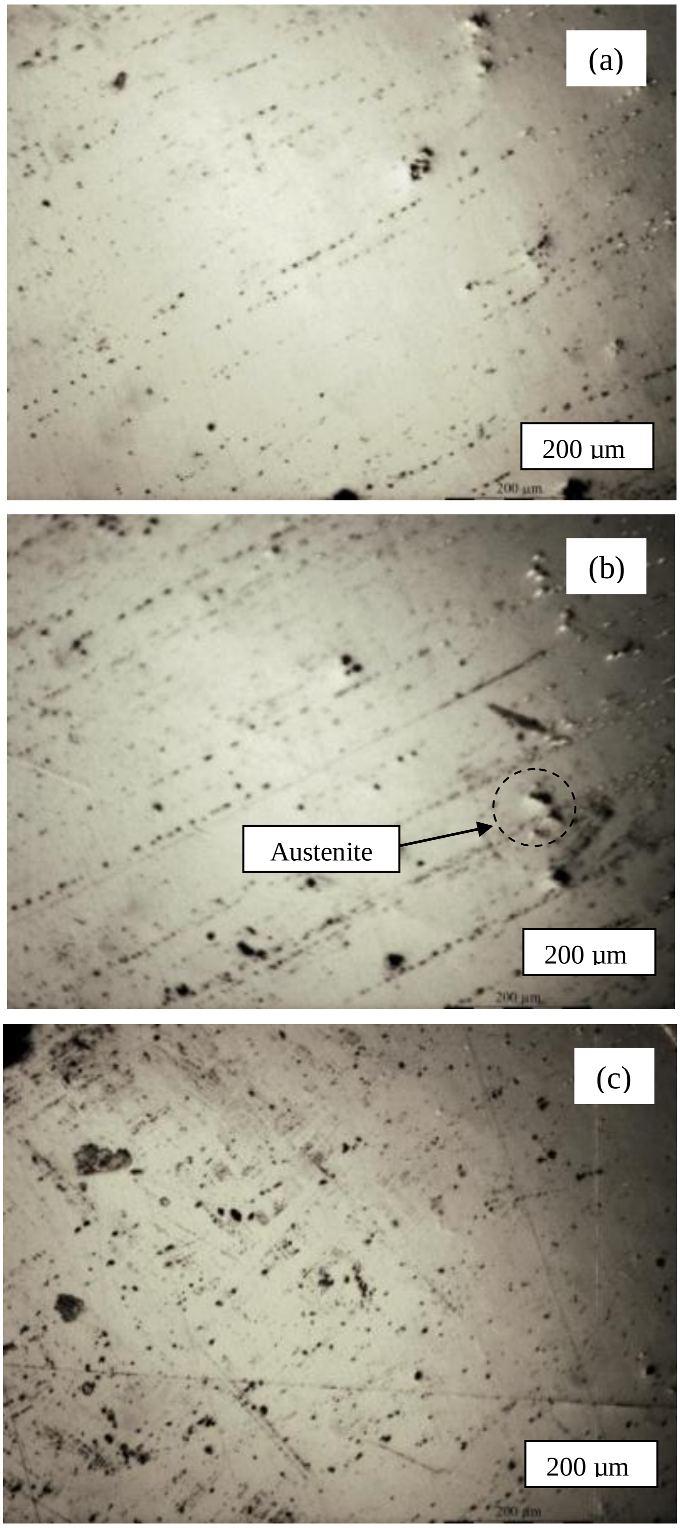

Figure 4.9: Micrographs showing the microstructure change in medium carbon steel joints before etching for same thickness of TWBs combination (a) base metal, (b) weld zone, and (c) HAZ

However, there has microstructure change present in the grain size contributing to the etching response. Figure 4.11 show there is a large size difference between grain in the HAZ of the thicker part and thinner part of the TWB (2 mm/3 mm). The grain size in the HAZ of the thinner part of the above TWB is larger than that of the thicker part as seen in Figure 4.11 (b). This is explained by the thermal cycle effects on the HAZs of the TWBs with different thickness. During welding, both parts of the TWB normally affected by the same heat source. The thinner part usually be heated up more quickly than the thicker part. However, the thinner part should have a longer recrystallization time than the thicker part. Therefore, the grain in thinner region is larger than that in the thicker region. Similar grain size found exist in TWBs of same thickness combination. This is because they have similar thermal cycle effects. The defects found in the weldment are porosity and cracks as shown in Figure 4.10 (b). Such defects can be critical if the part is exposed to cyclic stresses.

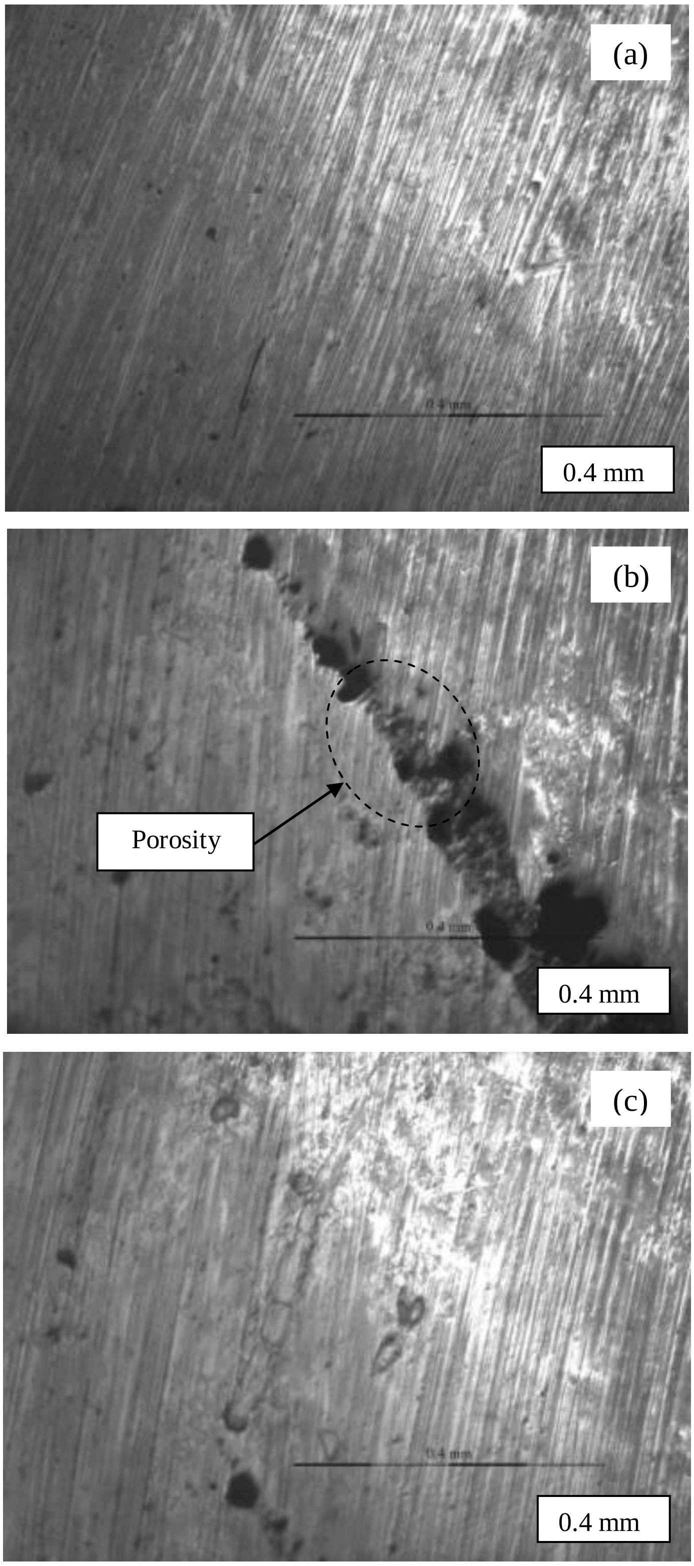

Figure 4.10: Micrographs showing the microstructure change in medium carbon steel joints after etching for same thickness TWB combination (a) base metal, (b) weld zone, and (c) HAZ

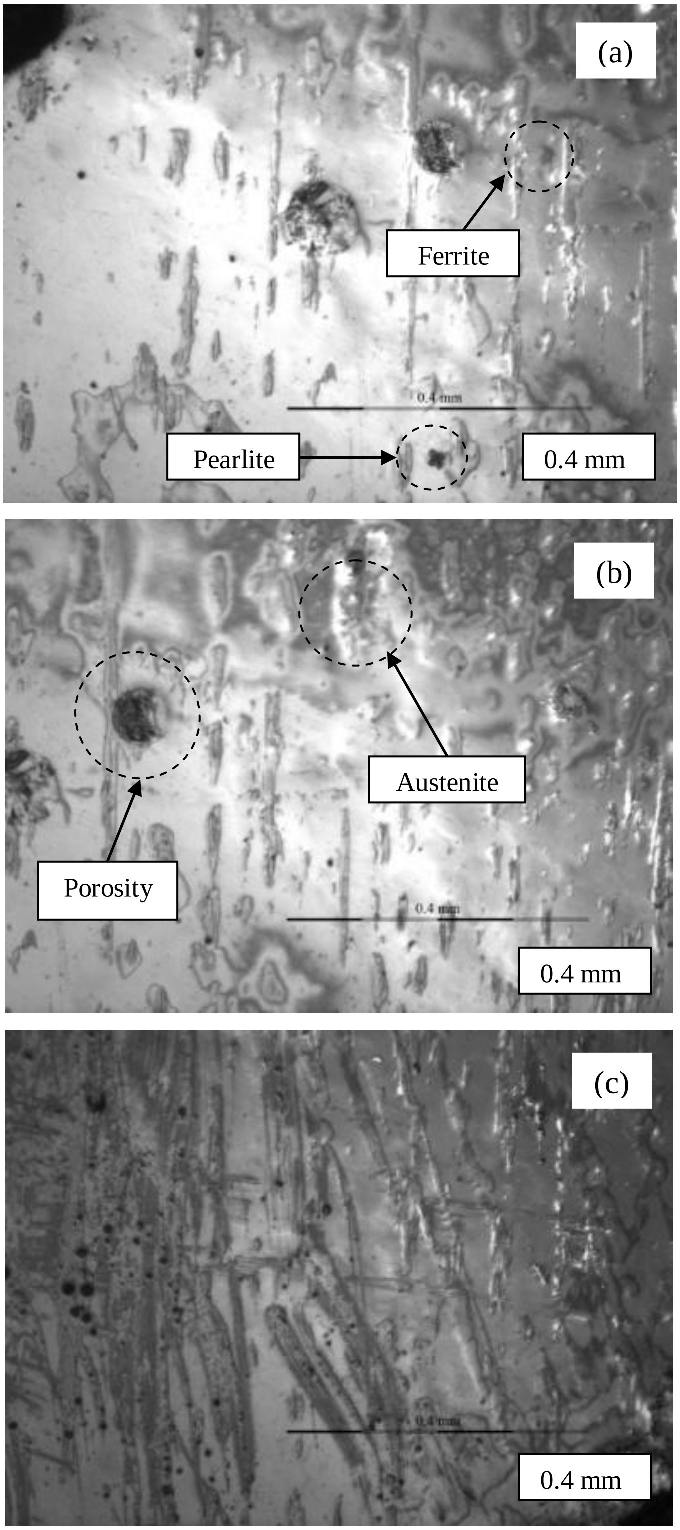

Figure 4.11: Micrographs showing the microstructure change in medium carbon steel joints after etching for different thickness TWB combination (a) base metal, (b) weld zone, and (c) HAZ

In order to study the effect of weld components, the joining are heated to a high temperature above the melting point of the parent metals and brought together to enable the components to coalesce. Grain size has a measurable effect on most mechanical properties including tensile strength and fatigue strength. Fine grain size has greater fatigue resistance toughness. The heat of welding operation is conducted into the parent metal such that in any weld joint there are three distinct areas, the weld metal in fusion welded joint, the HAZ in the parent material and the unaffected parent metal. The lower strength is acceptable and compensated in the weld metal.

4.7 SEM

After the fatigue test, the material was characterized by using SEM. The preparation procedure was more likely the same with the preparation for microstructure test in which the proper procedures were shown in Chapter 3. The fatigue crack initiation sites and crack propagation mechanisms were identified through examination of the fracture surfaces. Figure 4.12 below showed the microstructure in the base metals, weld zone and heat affected zone.

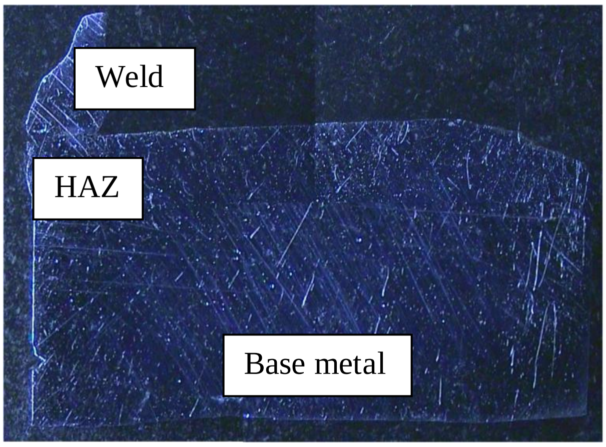

Figure 4.12: Cross section of the fracture specimen

The weld area is easily recognizable due to absence of large dimples that are present in the parent sheet area. In general the weld fracture surface is much smoother than that of the parent material. More detailed examination reveals that in the areas of the weld closer to the parent sheet much smaller dimples are present. The fracture surface demonstrates a brittle structure and only a small ductile region was observed. As shown in Figure 4.13 (b), the brittle fracture surface was relatively flat and smooth. As shown in Figure 4.13 (a), it exhibits ductile fracture characteristics and has a rough and irregular fracture surfaces which consists of lots of voids and small dimples. By moving towards the central regions of the weld, root or upper surface in the weld those dimples become shallower and are replaced by a much smoother surface, characteristics of sheared fracture. The finer dimple structure is a consequence of alteration of the second phase in the weld. In the parent metal, large particles act as nucleation sites for dormant voids, which result in large dimples. A few porosities were seen in the brittle fracture surface, which could be caused by the shielding gas as seen in Figure 4.13 (e). A larger number of smaller void-nuclei in particle-free weld producing a fine dimple structure.

The filler material and part of the base material meltdown during welding and form solidified weld metal, while the base material in the close region undergoes a transformation. HAZ formation is a result of an applied thermal cycle caused by the heat source movement as seen in Figure 4.13 (d) which necessary to melt the material. The effects of the thermal cycle diminish with distance from the fusion line. Materials close to the weld metal are heated almost to melting point and the high temperature produces a grain growth.

The grains structure in the melted weld area may form a desirable size and shape, while the grain structure of the surrounding HAZ may change to a less desirable shape and size and may cause cracking when welding on medium or high carbon steels. Often when welding hardenable steel the HAZ can harden to undesirable levels, while welding already hardened steel may result in a softened HAZ with loss of desired hardness.

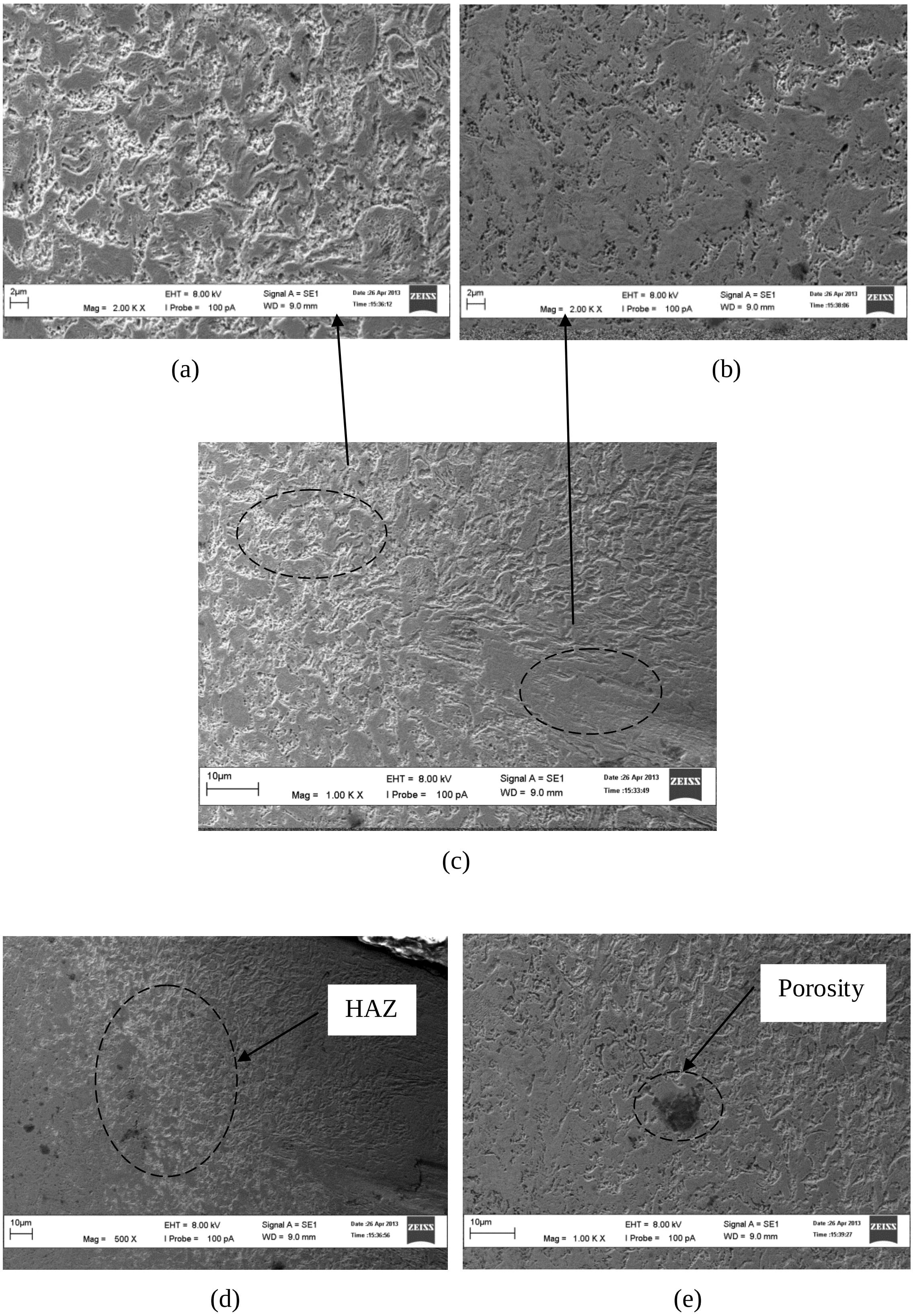

Figure 4.13: Typical SEM images of fatigue fracture surface (a) rough surface area, (b) smooth surface area, (c) transition zone, (d) HAZ and (e) defects

CHAPTER 5

CONCLUSION AND RECOMMENDATION

5.1 CONCLUSIONS

The objective of this study was to determine the effect of thickness ratio and loading direction on the tensile and fatigue behavior. From the results obtained, the following conclusions were drawn.

- In similar thickness TWB combination, the failure occurs on the base metal, while in the case of dissimilar thickness TWB, failure occurred in the thinner material. The failures occurred in the thinner parts (2 mm/3 mm) indicating that the formability of the TWBs is dependent on that of the thinner sheet. However, the tensile strength of the welded specimen to be lower than normal if it has defects.

- TWBs with two different weld line orientations such in 45 ^{o} and 90 ^{o} to the loading direction, the failure propagated parallel to the weld bead. Weld line oriented in 90^{o} to the loading direction was the best optimum angle for the current study.

- The microstructural examination of the weld cross sections revealed that the welds were experiencing defects such as porosity, crack and void. However, some of the welded specimens were free of any defects. This indicated that the welding parameters used for the TWBs are mostly appropriate. The defects presented on the specimens were likely due to the corrosion on the surface of specimen.

- Fatigue failures appear at the welds rather than in the base metal. The fatigue life of a material with welding is shorter than the life of base metal.

5.2 RECOMMENDATION

Although the present study was based on tailor welded blanks having similar and dissimilar material combinations but in terms of grades of steels, it was not really suitable. Similar study can be carried out by using the low carbon steels instead of medium carbon steels. Also, it is quite important to determine the suitable welding parameters and filler materials on the properties of the weld bead. The estimated parameters sometimes can bring effects to the properties weld bead. Although the majority of carbon steels used in fabricating parts are mild steel or low carbon and presents little difficulty in welding, some carbon steels that have more carbon such as tool steels, high alloy steels and cast iron require special procedures to prevent cracking and weld failure. Practically, only laser welding, mash welding and spot welding are have been shown to be practical in fulfilling the needs of a reliable, automated and serial production process for TWBs. This is because laser welding provides very good mechanical properties and formability than other welding processes for TWBs. Last but not least, we should put more attention and concentrated on the improvement of welding techniques to enhance joining and avoid poor weldabilty.

REFERENCES

Abdullah, K., Wild, P. M. Jeswiet, J. J. and Ghasempoor, A. 2001. Tensile testing for welding deformation properties in similar gage tailor welded blanks using the rule of mixtures. *Journal of Material Processing and Technology*, 112(1), 91-97.

Ahmetoglu, M. A., Brouwers, D., Shulkin, L., Taupin, L., Kinzel, G. L. and Altan, T. 1995. Deep drawing of round cups from tailor welded blanks. *Journal of Materials Processing Technology*, 53(3), 684-694.

Anand, D. 2004. *Formability and fatigue behavior of tailor (laser) welded blanks for automotive applications*. Master Thesis. Ryerson University, Canada.

Anand, D., Chen, D. L., Bhole, S. D., Andreychuk, P. and Boudreau, G. 2006. Fatigue behavior of tailor (laser) welded blanks for automotive applications. *Materials Science and Engineering A*, 420: 199-207.

Andrews, M. 2008. MIG welding and advantaged offered by this versatile process.source.theengineer.co.uk

Aristotile, R. and Fersini, M. 1999. Tailored blanks for automotive components. Evaluation of mechanical and metallurgical properties and corrosion resistance of laser welded joints. *Welding International*, 13(3), 16-25.

Auto/steel Partnership, 1995. Tailor welded blank design and manufacturing manual, Technical Report.

Auto/steel Partnership, 1998. Tailor welded blank design and manufacturing manual, Technical Report.

Babu, K. V., Narayanan, R. G., and Kumar, G. S. 2009. An expert system based on artificial neural network for predicting the tensile behavior of tailor welded blanks. *International Journal of Expert Systems with Applications*, 36: 10683-10695.

Balasubramanian, T. S., Balasubramanian, V. and Muthumanikkam, M. A. 2010. Effect of welding processes on fatigue properties of Ti-6Al-4V alloy joints. *International Journal of Mechanical and Materials Engineering*, 1: 3.

Baysore, K. K., Williamson, M. S., Adonyiadn, Y. and Milian, J. L. 1995. Laser beam welding and formability of tailored blanks. *Welding Research Supplement*, 345-352.

Chan, S. M., Chan, L. C. and Lee, T. C. 2001. Deformation mode analysis of forming limit diagrams for tailor welded blanks. *SAE Technical Paper*, 010092, 1-8.

Chan, S. M., Chan, L. C. and Lee, T. C. 2003. Tailor-welded blanks of different thickness ratios effects on forming limit diagrams. *Journal of Materials Processing Technology*, 132: 95-101.

Cheng, C. H. 2010. *Formability of tailor-welded blanks for rate-dependent materials*. Ph.D Thesis. Polytechnic University, Hong Kong.

Cheng, C. H., Chan, L. C., Tang, C. Y. and Chow, C. L. 2005. Determination of true stress-strain curve for the weldment of aluminum laser welded blanks. *Journal of Laser Application*, 17(3), 159-170.

Davies, R. W., Oliver, H. E., Smith, M. T. and Grant, G.J. 1999. Characterizing Al tailor welded blanks for automotive applications. *Journal of the Minerals Metals and Materials Society*, 51(11), 46-50

Ghoo, B. Y., Back, S. J., Keum, Y. T. and Kang, S. Y. 1998. Finite element analysis of tailored sheet forming processes considering laser welding zone. *Metals and Materials*, 4(4), 862-70.

Ghoo, B. Y., Keum, Y. T. and Kim, Y. S. 2001. Evaluation of the mechanical properties of welded metal in tailored steel sheet welded by CO2 laser. *Journal of Materials Processing and Technology*, 113(7), 692-698.

Ghoo, B.Y., Park, S. W. and Keum, Y. T. 2001. New forming limit diagram of laser tailored blank. *Journal of Strain Analysis*, 36(2), 143-152.

Groover, M. P. 2011. Principles of Modern Manufacturing, 4th ed., Wiley.

Kalpakjian, S. and Schmidt, S. 2004. Manufacturing Engineering & Technology. 5th ed., Prentice Hall.

Keeler, S. P. and Backofen, W. A. 1963. Plastic instability and fracture n sheets stretched over rigid punches. *Transactions of ASM*, 56, 25-48.

Kinsey, B., Liu, Z. and Cao, J. 2000. A novel forming technology for tailor-welded blanks. *Journal of Materials Processing Technology*, 99: 145-153.

Kleemola, H. J. and Kumpulainen, J. O. 1980a. Factors influencing the forming limit diagram: Part I – The experimental determination of the forming limits of sheer steel. *Journal of Materials Processing Technology*, 3, 289-302.

Kleemola, H. J. and Kumpulainen, J. O. 1980b. Factors influencing the forming limit diagram: Part II – Influence of sheet thickness. *Journal of Mechanical Working Technology*, 3 (3-4), 303-311.

Kridli, G. T., Friedman, P. A. and Sherman, A. M. 2000. Formability of aluminum tailor welded blanks. *SAE Technical Paper*, 010772.

Kusuda, H., Takasago, T. and Natsumi, F. 1997. Formability of tailored blanks. *Journal of Materials Processing Technology*, 71(1), 34-140.

Lazzarin, P., Rabino, E. and Zandonella Necca, D. 1995. Fatigue behavior of laser and resistance seam welds in the automotive industry. *Welding International*, 9(1), 165-172.

Lee, A. P., Feltham E. and Deventer, J. V. 1996. Tailor welded blank technology for automotive applications. *SAE Technical Paper*, 9660817: 91-102.

Li, J. 2010. *The effect of weld design on the formability of laser tailor welded blanks*. Degree Thesis. University of Waterloo, Canada.

Mendez, P. F. 2000. New trends in welding in the aeronautical industry. Massachusetts Institute of Technology, USA.

Oh, T. Y., Kwon, Y. K. Lee, C. J. and Kwak, D. S. 2000. The characteristics of fatigue strength in laser tailored welded blanking sheet metal. *Key Engineering Materials*, (183-187), 1321-1326.

Panda, S. K. and Kumar, D. R. 2008. Improvement in formability of tailor welded blanks by application of counter pressure in biaxial stretch forming. *Journal of Materials Processing Technology*, 204, 70-79.

Rhee, K. Y., Kwak, D. S. and Oh, T. Y. 2002. Fatigue behavior characterization of laser welded cold rolled sheet metal (SPCEN). *Journal of Materials Science*, 37(5), 1019-1025.

Saunders, F. I. 1994. *Forming of tailor-welded blanks*. Degree Doctorate of Philosophy Presentation, Ohio State University.

Saunders, F. I. and Wagoner, R. H. 1996. Forming of tailor welded blanks. *Metallurgical and Materials Transactions A*, 27(9), 2605-2616.

Shi, M. F., Pickett, K. M. and Bhatt, K. K. 1993. Formability issues in application of tailor welded blank sheets. *SAE Technical Paper*, 930278.

Smith, W. F. and Hashemi, J. 2006. Foundations of Materials Science and Engineering, 4th ed., McGraw Hill International.

Taylor, B. 1996. Formability testing of sheet metals. *ASM Handbook - v.14 Forming and Forging, ASM International*.

Tuler, F. R. et al., 1996. “An evaluation of the relative inherent dent resistance and stiffness of some steel and aluminium sheet materials for exterior closure panels, *International Engineering Conference Proceedings, Materials and Body Testing, IBEC Publications, Detroit, MI*, pp. 26-30.

Ultra Light Steel Auto Body Consortium, 1998. ULSAB Program Phrase 2 Final Report, *Technical Report*.

Wadell, W. and Davis, G. M. 1995. Laser welded tailored blanks in the automotive industry. *Welding and Metal Fabrication*, 105-108.

Wang, P. C. and Ewing, K. M. 1991. A comparison of fatigue strengths: Laser beam versus resistance spot welds. *Welding Journal*, 70(10), 43-47.

APPENDIX

A1

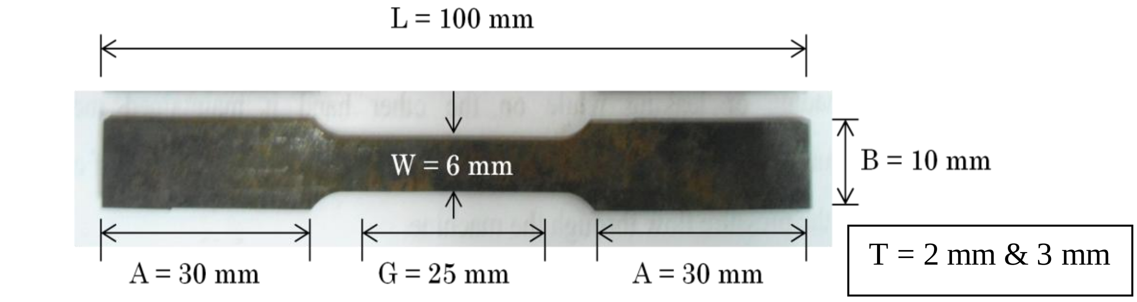

ASTM E8

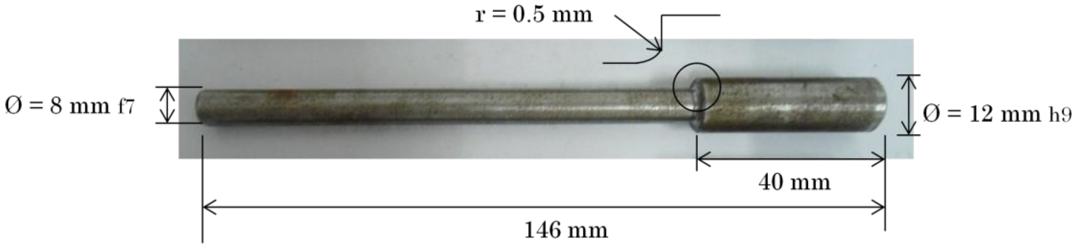

ASTM E467

A2

FOUNDRY LABORATORY
FACULTY OF MECHANICAL ENGINEERING
UNIVERSITI MALAYSIA PAHANG

Chemical Results

Date: 05/11/2012

Sample ID:		Material:	steel
Customer:	angelina	Dimension:	
Commision:		Filter metals:	
Lab-no.:		Heat treatment:	
Reference no.:		Heat-no:	

Spectrometer Foundry-MASTER Grade :

	Fe	C	Si	Mn	P	S	Cr	Mo
1	95,2	0,412	0,328	0,662	0,327	> 0,150	0,178	0,0868
2	95,2	0,486	0,505	1,12	0,162	> 0,150	0,239	0,0634
3	95,4	0,548	0,569	1,19	0,103	> 0,150	0,240	0,0523
4	96,3	0,439	0,344	0,985	0,112	> 0,150	0,209	0,0446
5	95,6	0,520	0,579	1,29	0,0999	> 0,150	0,314	0,0694
6	96,0	0,390	0,514	1,18	0,0866	> 0,150	0,289	0,0641
7	96,6	0,505	0,336	1,23	0,0747	> 0,150	0,227	0,0347
Ave	95,8	0,471	0,454	1,09	0,138	> 0,150	0,242	0,0593

	Ni	Al	Co	Cu	Nb	Ti	V	W
1	0,484	0,0405	0,405	0,109	0,0863	0,0628	0,0288	0,954
2	0,450	0,0479	< 0,0100	0,128	0,0816	0,0573	0,0243	0,805
3	0,385	0,0452	< 0,0100	0,117	0,0664	0,0541	0,0218	0,737
4	0,323	0,0344	< 0,0100	0,128	0,0594	0,0445	0,0149	0,555
5	0,329	0,0369	< 0,0100	0,120	0,0607	0,0450	0,0192	0,503
6	0,313	0,0342	< 0,0100	0,195	0,0570	0,0414	0,0194	0,397
7	0,228	0,0413	< 0,0100	0,0874	0,0449	0,0342	0,0101	0,256
Ave	0,359	0,0401	0,0605	0,126	0,0652	0,0485	0,0198	0,601

	Pb
1	0,241
2	0,213
3	0,192
4	0,144
5	0,138
6	0,121
7	0,0860
Ave	0,162

Foundry Laboratory
Faculty of Mechanical Engineering
Universiti Malaysia Pahang
26600 Pekan, Pahang, MALAYSIA
Tel: +604242213 / 2270 / 2317
Fax: +6094242202
Website: http//:fkm.ump.edu.my

Test by: Verify by:

A3

UNIVERSITI MALAYSIA PAHANG

FACULTY OF MECHANICAL ENGINEERING

TEST REPORT

Method description

Sample description

STRESS STRAIN CURVE

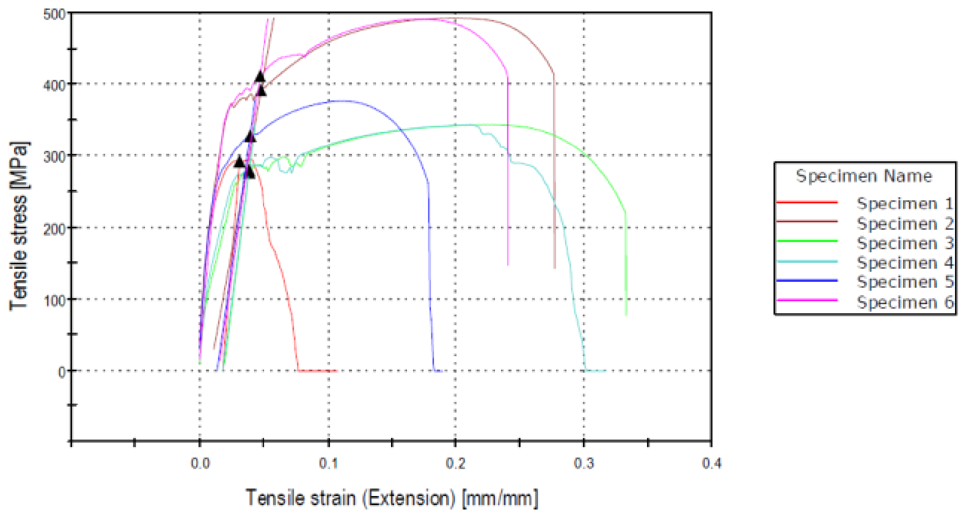

	Specimen label	Tensile stress at Yield (Slope threshold 0.02 %) [MPa]	Modulus (Automatic) [MPa]	Tensile stress at Tensile strength [MPa]	Tensile stress at Break (Standard) [MPa]	Tensile strain (Extension) at Break (Standard) [mm/mm]
1	Specimen 1	292.36	22,502.07	292.43	0.11	0.11
2	Specimen 2	391.79	9,851.68	491.88	143.45	0.28
3	Specimen 3	277.36	14,019.41	343.69	77.66	0.33
4	Specimen 4	280.24	13,586.29	342.45	0.25	0.32
5	Specimen 5	328.53	12,806.22	376.06	-0.09	0.19
6	Specimen 6	411.71	12,651.19	489.92	147.81	0.24

4/2/2013 11:49:38 PM

A4

General recommendation for turning operation

TABLE 23.4

General Recommendations for Turning Operations

Workpiece material	Cutting tool	General-purpose starting conditions: Depth of cut, mm (in.)	General-purpose starting conditions: Feed, mm/rev (in./rev)	General-purpose starting conditions: Cutting speed, m/min (ft/min)	Range for roughing and finishing: Depth of cut, mm (in.)	Range for roughing and finishing: Feed, mm/rev (in./rev)	Range for roughing and finishing: Cutting speed, m/min (ft/min)
Low-C and free machining steels	Uncoated carbide	1.5–6.3 (0.06–0.25)	0.35 (0.014)	90 (300)	0.5–7.6 (0.02–0.30)	0.15–1.1 (0.006–0.045)	60–135 (200–450)
	Ceramic-coated carbide	"	"	245–275 (800–900)	"	"	120–425 (400–1400)
	Triple-coated carbide	"	"	185–200 (600–650)	"	"	90–245 (300–800)
	TiN-coated carbide	"	"	105–150 (350–500)	"	"	60–230 (200–750)
	Al_2O_3 ceramic	"	0.25 (0.010)	395–440 (1300–1450)	"	"	365–550 (1200–1800)
	Cermet	"	0.30 (0.012)	215–290 (700–950)	"	"	105–455 (350–1500)
Medium and high-C steels	Uncoated carbide	1.2–4.0 (0.05–0.20)	0.30 (0.012)	75 (250)	2.5–7.6 (0.10–0.30)	0.15–0.75 (0.006–0.03)	45–120 (150–400)
	Ceramic-coated carbide	"	"	185–230 (600–750)	"	"	120–410 (400–1350)
	Triple-coated carbide	"	"	120–150 (400–500)	"	"	75–215 (250–700)
	TiN-coated carbide	"	"	90–200 (300–650)	"	"	45–215 (150–700)
	Al_2O_3 ceramic	"	0.25 (0.010)	335 (1100)	"	"	245–455 (800–1500)
	Cermet	"	0.25 (0.010)	170–245 (550–800)	"	"	105–305 (350–1000)
Cast iron, gray	Uncoated carbide	1.25–6.3 (0.05–0.25)	0.32 (0.013)	90 (300)	0.4–12.7 (0.015–0.5)	0.1–0.75 (0.004–0.03)	75–185 (250–600)
	Ceramic-coated carbide	"	"	200 (650)	"	"	120–365 (400–1200)
	TiN-coated carbide	"	"	90–135 (300–450)	"	"	60–215 (200–700)
	Al_2O_3 ceramic	"	0.25 (0.010)	455–490 (1500–1600)	"	"	365–855 (1200–2800)
	SiN ceramic	"	0.32 (0.013)	730 (2400)	"	"	200–990 (650–3250

(Continued)

Source: Kalpakjian, S. and Schmid, S. R. (2004)

A5

Gantt Chart for FYP 1

Week Activity	1	2	3	4	5	6	7	8	9	10	11	12	13	14
Collect the data														
Discuss on the materials and method used														
Prepare the materials and apparatus														
Fabricate the specimens														
Prepare the final draft proposal														
Correct and evaluate on the final draft														
Submit the final draft report														
Present the draft report														

A6

Gantt Chart for FYP 2

Week / Activity	1	2	3	4	5	6	7	8	9	10	11	12	13	14	15
Conduct the research															
Fabricate the specimens															
Work on the testing															
Collect the data															
Analyze the data															
Write up the report															
Correct and evaluate the final report															
Present the final report															
Submit the final report															